
TOWARDS A LONG-TERM CONTROL OF COVID-19 AT LOW CASE NUMBERS

Sebastian Contreras¹, Jonas Dehning¹, Sebastian B. Mohr¹, F. Paul Spitzner¹, and Viola Priesemann^{1,2*}

¹Max Planck Institute for Dynamics and Self-Organization, Am Faßberg 17, 37077 Göttingen, Germany.

²Department of Physics, University of Göttingen, Friedrich-Hund-Platz 1, 37077 Göttingen, Germany.

All authors contributed equally.

Abstract

As SARS-CoV-2 is becoming endemic, a sustainable strategy to manage the pandemic is needed, especially when facing a steep wave. We identified a metastable regime at low case numbers, where test-trace-and-isolate (TTI) together with moderate contact reduction is sufficient to control the spread. However, this control is lost once case numbers overwhelm the limited TTI capacity. Beyond that tipping point, increasingly more infectious individuals remain undetected, generating a self-accelerating spread. To reestablish control, a lockdown (circuit breaker) has to strike a delicate balance between duration, stringency, and timeliness; otherwise, lockdowns are ineffective, or their effect is soon lost. However, once reestablishing control at low case numbers, no additional lockdowns are necessary. In the long-term, immunity and large-scale testing will further facilitate the control of COVID-19.

*viola.priesemann@ds.mpg.de

Contents

1	Introduction	3
2	Results	3
2.1	Model Overview	3
2.2	A metastable regime of COVID-19 at low case numbers can be achieved with moderate contact reduction.	4
2.3	The equilibrium value of daily new infections depends on the influx and the reduction of contagious contacts.	5
2.4	If case numbers exceed the capacity of testing and tracing, the spread gets out of control and self-accelerates.	6
2.5	Lockdowns can re-establish control once the spread got out of control — if implemented correctly.	6
2.6	Long-term perspective: Repeated lockdowns are not required to maintain control over the COVID-19 spread	9
3	Discussion	10
3.1	Recent COVID-19 spreading dynamics in Europe may reflect exceeded TTI capacity	11
3.2	Strategies to face COVID-19 differ among countries	11
3.3	Central parameters of our model	12
3.4	Conclusion and Outlook	12
S1	Methods	16
S1.1	Spreading Dynamics	16
S1.2	Parameter Choices and Scenarios	17
S1.3	Testing-and-Tracing strategies	17
S1.4	Lockdown modelling	17
S1.5	Model Equations	18
S1.6	Initial conditions	18
S1.7	Effect of delays and capacity limit on the effectiveness of TTI strategies	19
	S1.7.1 Limited testing capacity leading to lower testing rates	19
	S1.7.2 Modelling the number of traced individuals	19
	S1.7.3 Individuals becoming infectious or being tested by the time of tracing	20
S1.8	Central epidemiological parameters that can be observed	20
S1.9	Numerical calculation of solutions and critical values.	21
S2	Supplementary Notes	23
S2.1	Strategies to face COVID-19 differ among countries.	23
S2.2	On the incorporation of random testing in the TTI scheme	24
	S2.2.1 Number of cases observable through testing N^{test}	25
	S2.2.2 Number of cases observable through contact-tracing N^{traced}	25
S2.3	Linear stability analysis and uncertainty propagation	26

1 Introduction

As SARS-CoV-2 is becoming endemic and knowledge about its spreading is accumulated, it becomes clear that neither global eradication nor herd immunity is achieved soon. Eradication is hindered by the worldwide prevalence and by asymptomatic spreading. Reaching herd immunity without an effective vaccine or medication would take several years and cost countless deaths, especially among the elderly. Moreover, long-term effects ("long COVID") are surfacing [1–5]. Hence, we need long-term, sustainable strategies to contain the spread of SARS-CoV-2. The common goal, especially in countries with an aging population, should be to minimize the number of infections and, thereby, allow reliable planning for individuals and the economy – while not constraining individuals' number of contacts too much. Intuitively, a regime with low case numbers would benefit not only public health and psychological well-being but likely also profits economy [6, 7].

The containment of SARS-CoV-2 is challenging: Many infections originate from asymptomatic or pre-symptomatic cases [8], rendering mitigation measures difficult. Therefore, within test-trace-and-isolate (TTI) strategies, mitigation effects achieved by symptomatic testing are restricted, but contact tracing can partially prevent further transmissions from non-symptomatic individuals. Additional challenges are the potential influx of SARS-CoV-2 infections brought in by travelers from abroad, imperfect quarantine, and limited compliance. Last, countries' capacity to perform test-trace-and-isolate is limited, which changes spreading dynamics depending on case numbers levels. Understanding these dynamics is thus crucial for an informed policy decisions.

We investigated how to harness test-trace-and-isolate (TTI) strategies in combination with moderate contact reduction to control the pandemic at low case numbers. We found that the limited TTI capacity induces a metastable regime of SARS-CoV-2 spread at *low case numbers*: In this regime, case numbers are only stable under a certain threshold determined by TTI capacity and are otherwise unstable (Sec. 2.2). If stable, the resulting level of case numbers depend on the influx of infections and the reduction of contacts (Sec. 2.3). Next, we demonstrate that if the spread gets out of control nonetheless (as with the second wave in many European countries), it leads to a self-accelerating increase of case numbers (Sec. 2.4). In this case, we show how to design an efficient single circuit breaker or lockdown to reach low case numbers again, where TTI can operate within its capacity and serves as an effective control measure (Sec 2.5). Our results indicate that a few weeks with substantial contact reduction are typically sufficient to reach this low case numbers regime. Once reached, contact restrictions can be loosened. However, if measures are lifted too quickly, or are not implemented stringently enough, then the efforts and costs of such circuit breakers are soon lost, and a novel reset becomes necessary. Last, we outline strategies for a long-term stable regime with moderate contact reductions (Sec. 2.6) and discuss our theoretical results in view of the development of case numbers and the mitigation policies of countries throughout the world.

2 Results

2.1 Model Overview

We developed an SEIR-type compartmental model [9–12] to investigate mitigation strategies and long-term control for COVID-19 (for a graphical representation of the model see Fig. S1). In the model, we incorporated the central challenges of SARS-CoV-2 mitigation: asymptomatic carriers of the virus, imperfect contact tracing and quarantining, and delays in testing, tracing, and case-reporting [12]. Importantly, as case numbers increase, available tests may not suffice to test all suspected cases, and the personnel at the health authorities may become unable to trace further contacts. Thus, we modeled a limited test-trace-and-isolate (TTI) capacity beyond which tests are performed at a lower rate, and no further contacts can be traced.

A central parameter in the model is the effective reduction of contagious contacts k_t relative to pre-COVID-19. More precisely, k_t quantifies the reduction in (potentially) contagious contacts a person produces. This reduction of contacts accounts for both healthy individuals and those infected who are not aware of being infectious. Contributions are obviously from contact reduction, but also from enhanced hygiene, mandatory face-mask policies, frequent ventilation of closed spaces, and shift to outside gatherings, among other precautionary measures. As we assume that the latter measures are relatively fixed, direct contact reduction remains the central free variable, which is also the one tuned during lockdowns. Thus, while we can only estimate roughly how much each measure contributes to the overall contact reduction k_t , we can still clearly read off the model how strongly k_t needs to be reduced in a lockdown or circuit breaker to regain stability within just a few weeks – and to maintain stability afterward.

All model parameters are listed in Table S1. Epidemiological parameters are based on the available SARS-CoV-2 literature [13–17], whereas parameters related to test-trace-and-isolate policies and lockdowns are obtained from German and European situation reports. A interpretation of those parameters is discussed in section 3.3. Our code is available at https://github.com/Priesemann-Group/covid19_research/tree/master/circuit_breaker, and an interactive platform to explore alternative scenarios and parameters will be soon available (in preparation, the link will be on GitHub once it is online).

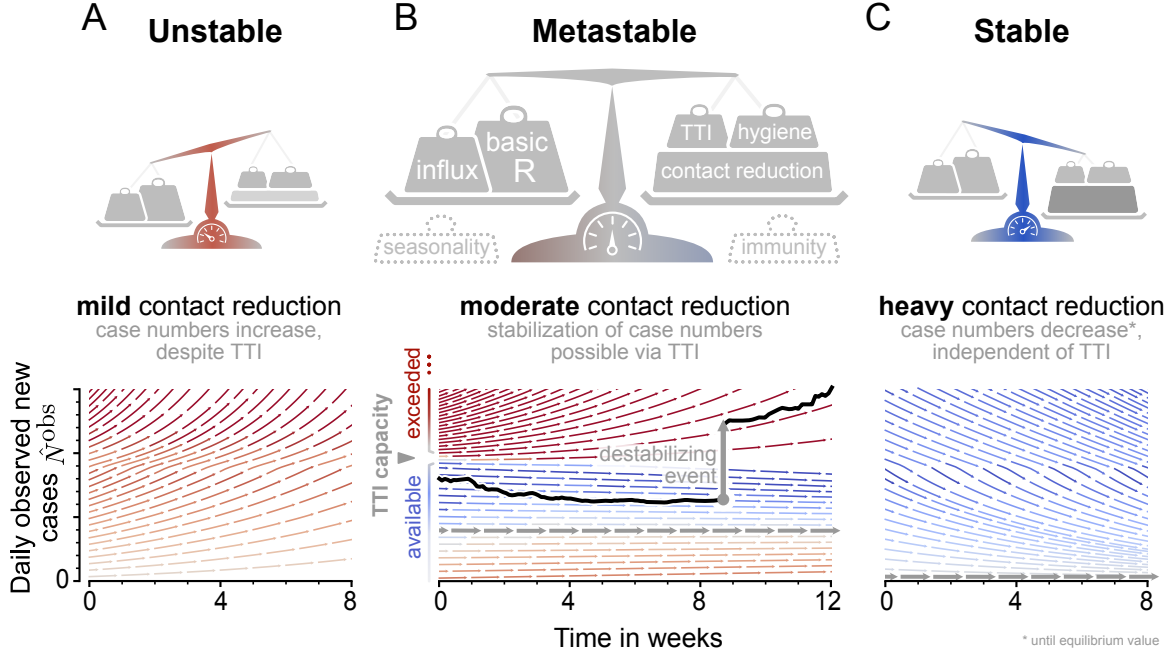


Figure 1: **The dynamics of daily new case numbers depend on the balance between destabilizing and stabilizing contributions, but also on the level of case numbers itself.** Disease spread is destabilized by the basic reproduction number R_0 and the external influx of infections (and possibly seasonality). On the other hand, the spread can be stabilized by various contributions, including increased hygiene, test-trace-isolate strategies (TTI), contact reduction, but also immunity. We investigated how specifically contact reduction k_0 and limited TTI capacity determine the stabilization of case numbers. (A) Assuming only mild contact reduction ($k_0 = 20\%$ compared to pre-COVID), TTI is not sufficient to prevent increasing case numbers — even when TTI capacity is still available. Hence, case numbers are increasing. (B) At moderate contact reduction ($k_0 = 40\%$), a metastable state emerges (bold horizontal arrows) to which case numbers converge — if case numbers do not exceed the TTI capacity. However, destabilizing events (as, e.g., a sudden influx of infections), can push a previously stable system above the TTI capacity and lead to an uncontrolled spread (black line as an example). (C) Assuming heavy contact reduction ($k_0 = 60\%$), case numbers decrease even if the TTI capacity is exceeded. (*) Case numbers decrease until they reach a low equilibrium point (bold horizontal arrows); due to a constant small external influx of cases ($\Phi = 1$ case/day), the equilibrium is not at zero.

2.2 A metastable regime of COVID-19 at low case numbers can be achieved with moderate contact reduction.

In addition to the two classical scenarios of a pandemic — an eradication or a general spreading throughout the population, potentially with subsequent immunity — our model displays a metastable regime, where case numbers very early on converge reliably to low values (Fig. 1). The precise level of case numbers depends on various contributions, such as the basic reproduction number R_0 , the influx of new infections Φ_t and seasonality, but also precautionary measures (hygiene, masks, ventilation), test-trace-and-isolate (TTI) strategies, and contact reduction. When considered jointly, all the contributions give rise to the effective reproduction number \hat{R}_t^{eff} , which can be significantly lower than the basic reproduction number ($R_0 \approx 3.3$ for SARS-CoV-2 [14, 18–20]).

We focused on how contact reduction k_t and the number of daily new cases \hat{N}^{obs} together affect the stability of the system. Contact reduction can be achieved effectively by non-pharmaceutical interventions (NPIs); it

is the main control parameter that determines whether the system is unstable, metastable, or stable (Fig. 1). We quantify this effect by the factor k_t , the *reduction of contagious contacts compared to the pre-COVID-19 times*, which models the decrease in viral transmission via behavior. If the contact reduction k_t is mild, case numbers still grow exponentially, and the system is unstable (Fig. 1 A). In contrast, if the contact reduction is strong and (together with hygiene and TTI) outweighs the drive by the basic reproduction number, then case numbers decrease to an equilibrium at very low case numbers, and the system is stable (Fig. 1 C). If the contact reduction is moderate (and just-about equilibrates the drive by the basic reproduction number), we find a metastable regime: The spread is stabilized *if* overall case numbers are sufficiently low to enable fast and efficient TTI (Fig. 1 B). However, if the limited TTI capacity is overwhelmed, TTI starts to miss cases and its contribution to reducing case numbers is weakened. This presents a tipping point, beyond which the spread self-accelerates [12].

2.3 The equilibrium value of daily new infections depends on the influx and the reduction of contagious contacts.

When contacts are sufficiently reduced, the system is stable or metastable, and case numbers can reach an equilibrium. If in equilibrium, the precise *level* of daily new infections $\hat{N}_\infty^{\text{obs}}$ directly depends on the reduction of contagious contacts k_t and the external influx of new cases Φ_t (Fig. 2). The $\hat{N}_\infty^{\text{obs}}$ increases steeply (it diverges) when the contact reduction k_t approaches the tipping point to unstable dynamics. Such a divergence near a critical point k_t^{crit} is a general feature of continuous transitions between stable and unstable dynamics [21, 22]. As a rule of thumb, in a very simplified model, $\hat{N}_\infty^{\text{obs}}$ would be proportional to Φ_t and diverge when k_t approaches its critical value k_t^{crit} from above: $\hat{N}_\infty^{\text{obs}} \propto \Phi_t / (k_t - k_t^{\text{crit}})$ [22].

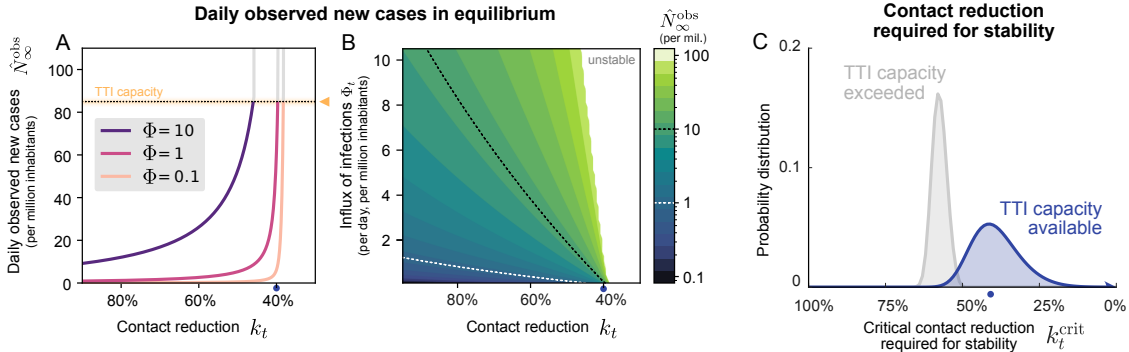


Figure 2: **In the stable and metastable regimes, daily new cases approach an equilibrium value $\hat{N}_\infty^{\text{obs}}$ that depends on contact reduction k_t and external influx of new cases Φ_t .** (A) The equilibrium value $\hat{N}_\infty^{\text{obs}}$ increases steeply with lower k_t and then destabilizes when surpassing a critical value k_t^{crit} . Thus, contact reduction has to be sufficiently strong to keep the case numbers within TTI capacity. A certain degree of external influx Φ_t can be compensated, but in general, Φ_t can put stability at risk. $\Phi_t = 1$ one daily new case per million is our default parameter for the influx. (B) The $\hat{N}_\infty^{\text{obs}}$ is below 10 for a large fraction of parameter combinations, k_t and Φ_t , thus well below the capacity limit of TTI. (C) The critical value k_t^{crit} , which marks the transition between stable and (meta)stable spread; thus k_t^{crit} displays the minimal contact reduction that is required to control the spread (and stabilize case numbers). If case numbers are below the TTI capacity limit, a contact reduction of at least $k_t^{\text{crit}} = 39\%$ is required for stabilization (blue). If case numbers, however, are above the TTI limit, stronger contact reduction is necessary for stabilization ($k_t^{\text{crit}} = 58\%$, gray). Confidence intervals originate from error propagation of the uncertainty of the underlying model parameters. All model parameters are listed in Table S3 and the full uncertainty analysis is in Fig. S3.

In the metastable regime, the spread is stabilized as long as case numbers stay below the test-trace-and-isolate (TTI) capacity of local health authorities, and k_t is sufficiently low. However, a robust control of the pandemic requires maintaining a sufficient safety-margin from the tipping point, and the subsequent transition to instability – for two main reasons: First, small fluctuations in k_t , Φ_t (or other model variables) could easily destabilize the system. Second, compared to the critical value k_t^{crit} (i.e. the minimum contact reduction required for stability), a further reduction by just 5% leads to significantly lower case numbers (Fig. 2 A). In fact, case numbers are well below 10 daily new infected per million in the vast majority of the stable

parameter regime (Fig. 2 B, lower left region). Thus, already with moderate contact reduction, a regime of case numbers clearly below 10 per million can be stabilized well.

The specific contact reduction that is required to achieve an equilibrium depends on the TTI effectiveness. If case numbers are sufficiently low and thus the TTI is fast and effective, then the required contact reduction is $k_t^{\text{crit}} = 39\%$ (95% confidence interval (CI): [24, 53]%). However, if case numbers exceed the TTI capacity limit, a considerably stronger contact reduction of $k_t^{\text{crit}} = 58\%$ (95% CI: [53, 62]%) is required for stabilization (Fig. 2 C and Table S3). Precise values depend on the specific parameters of the model, and each parameter carries its own uncertainty. We propagated these uncertainties and thereby obtained the above uncertainty estimates (Supplementary Note S2.3).

We investigated the results are affected by various model parameter, including imperfect quarantine, asymptomatic carriers (which are harder to detect), and the respective delays associated with incubation, testing and contact tracing, and case-reporting delays (Supplementary Fig. S3). Among all parameters, the ones that have the highest impact on mitigation are (i) a sufficiently strict quarantine and isolation — otherwise, infection chains are not stopped despite isolation; (ii) the specific fraction of asymptomatic individuals — because while not detected, these cases strongly contribute to the inadvertent transmission; and (iii) the availability of symptom-driven testing — because the earlier a symptomatic person is detected, the earlier their (potentially asymptomatic) infected contacts can be identified and subsequently quarantined. However, even with TTI, precautionary measures and clear contact reductions remain necessary for containment, and therefore, for avoiding an uncontrolled spread.

2.4 If case numbers exceed the capacity of testing and tracing, the spread gets out of control and self-accelerates.

If case numbers surpass the capacity limit, the system crosses a tipping point, and the spread gets out of control. This is reflected in the following observables (Fig. 3):

First, the increase in daily new *observed* cases \hat{N}_t^{obs} becomes steeper, growing even faster than the previous exponential growth (Fig. 3 A, full versus faint line). In the simulated scenario, we assumed a slight increase in case numbers over a few months, as observed in Germany and many other European countries throughout the summer (Fig. 6). Here, case numbers increased because the contact reduction of $k_t = 20\%$ is not sufficient to ensure stability. When case numbers surpass the TTI capacity, the spread self-accelerates because increasingly more contacts are missed. Importantly, in this scenario, the accelerated spread arises solely because of exceeding the TTI limit — thus without any underlying behavior change among the population.

Second, the observed reproduction number \hat{R}_t^{obs} , which had been only slightly above the critical value of unity, increased to about $\hat{R}_t^{\text{obs}} = 1.2$ (Fig. 3 B). This shows that not only case numbers but even the reproduction number itself \hat{R}_t^{obs} increases after case numbers surpass the TTI limit. The above reflects a gradual loss of control over the spread and explains the faster-than-exponential growth of case numbers. The initial dip in \hat{R}_t^{obs} is a side-effect of the limited testing: as increasingly many cases are missed, the observed reproduction number reduces transiently. This dip is also visible in Fig. 1 at the TTI limit.

Third, compared to the infectious individuals who are quarantined I^Q , the number of infectious individuals who are hidden I^H (i.e. those who are not isolated or in quarantine) increases disproportionately (Fig. 3 C). The hidden infectious individuals are the silent drivers of the spread as they, unaware of being infectious, inadvertently transmit the virus. This implies a considerable risk, especially for vulnerable people. At low case numbers, the TTI system is capable to compensate the hidden spread, because it uncovers hidden cases through contact tracing. However, at high case numbers, the TTI slows down; it may become “slower than the viral spread”, and starts to fall short of its purpose to quarantining contacts before they become spreaders.

Fourth, and related, the so-called dark figure, estimated in the model as the ratio between hidden and detected infected (I^H/I^Q), increases considerably once TTI capacity is surpassed. The dark figure is not directly observable from reported case numbers in real-world settings, however, our model suggests that beyond the TTI limit, the fraction of hidden carriers and spreaders of the virus among the population grows (Fig. 3 D).

2.5 Lockdowns can re-establish control once the spread got out of control — if implemented correctly.

Once the number of new infections has overwhelmed the TTI system, re-establishing control can be challenging. A recent suggestion is the application of a circuit breaker [23–25], a short lockdown to significantly lower the

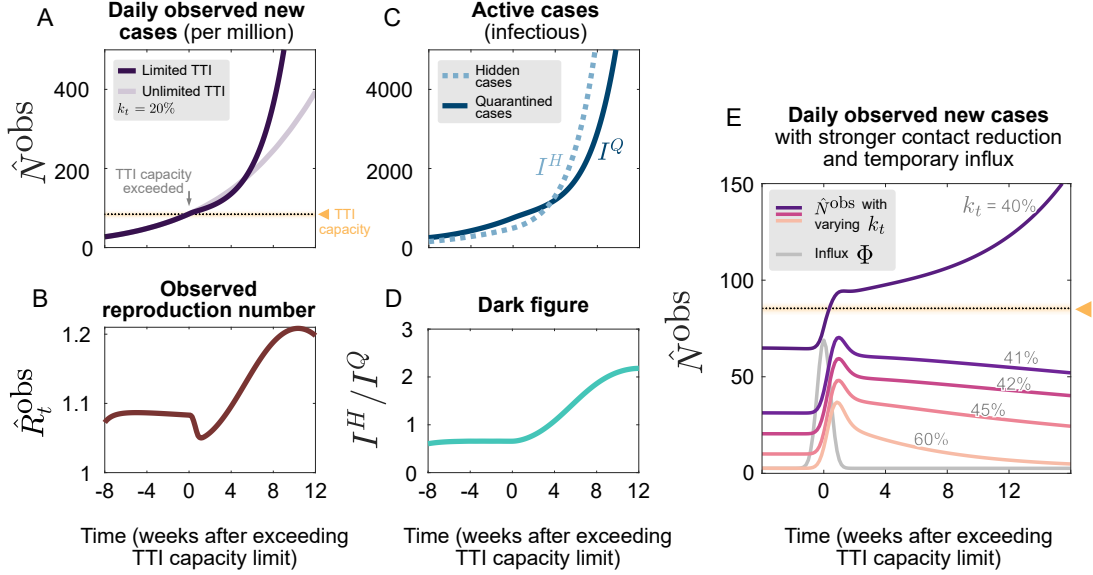


Figure 3: **Exceeding tracing capacity has an observable effect in case numbers, accounting for several unobserved changes.** (A-D) We consider a scenario with insufficient contact reduction ($k_t = 20\%$): At $t = 0$, the TTI capacity limit is exceeded which leads to (A) observed case numbers \hat{N}^{obs} growing faster than the previously observed exponential growth (dark versus light line, respectively), and (B) the observed reproduction number \hat{R}_t^{obs} steeply increasing after a transient drop. (The transient drop reflects the slow down in testing). (C) This breakdown of TTI also leads to a strong increase in the hidden (i.e. not or not yet detected) infectious pool I^H , which becomes larger than the quarantined infectious pool I^Q . (D) Consequently, the dark figure, calculated as the ratio between the two pools I^H/I^Q , increases. Both the increase in I^H/I^Q and \hat{R}_t^{obs} , make controlling the spread increasingly difficult after surpassing the TTI limit. (E) We further consider scenarios in the metastable regime. Here, the baseline influx is the same as in panel A, but the contact reduction is larger ($k_t \geq 40\%$, as indicated in the figure). This renders the dynamics stable below the TTI limit. Then, one large temporary influx event (super-spreading event, or end of holidays) is added at $t = 0$ (gray line): In this example, already a contact reduction of $k_t = 40\%$ or $k_t = 41\%$ makes the difference whether case numbers are already low before the influx event, and subsequently an influx event is absorbed by the available TTI capacity — or not. Thus, if case numbers are already near the TTI limit, even a moderate temporary influx can destabilize the system.

number of daily new infections. However, in the following we show that it has to be strong enough and long enough to show effect, and even after the circuit breaker, moderate or strong contact reductions have to be maintained.

Already during the first wave, lockdowns have proven capable to lower case numbers by a factor 2 or more every week (corresponding to an effective reproduction number of $\hat{R}_t^{\text{eff}} \approx 0.7$). With the knowledge we now have acquired about the spreading of SARS-CoV-2, more targeted restrictions may yield a similarly strong effect. However, one central challenge remains: Due to the delays between contagion and case-report, effects of interventions start to be observable only 1-2 weeks after initiating the lockdown. Hence, in practice, it is necessary to reevaluate a strategy after that waiting time.

Inspired by the lockdowns installed in Germany and many other countries, we assume a default lockdown that starts two weeks after case numbers exceed the TTI capacity limit. The lockdown has a default duration of four weeks and an effective reduction of contagious contacts by $k_{\text{LD}} = 75\%$ relative to the pre-COVID-19 (which translates to $\hat{R}_t^{\text{eff}} \approx 0.85$). After the lockdown, a moderate contact reduction ($k_{\text{nLD}} = 40\%$) is maintained. As lockdowns typically comprise both a strong contact reduction and travel restrictions, we also reduce the external influx Φ_t by a factor 10 during the lockdown. By varying the parameters of this default lockdown, we show in the following that the lockdown strength, duration and starting time determine its success in regaining control. The complete dependency is depicted in Fig. 4 G and H.

The duration of a lockdown determines whether or not a stable regime is reached. In our scenario, a lockdown duration of four weeks is sufficient to reach the stable regime (Fig. 4 A). However, if lifted too early (before completing four weeks), then case numbers will rise again shortly after easing the lockdown. The shorter an

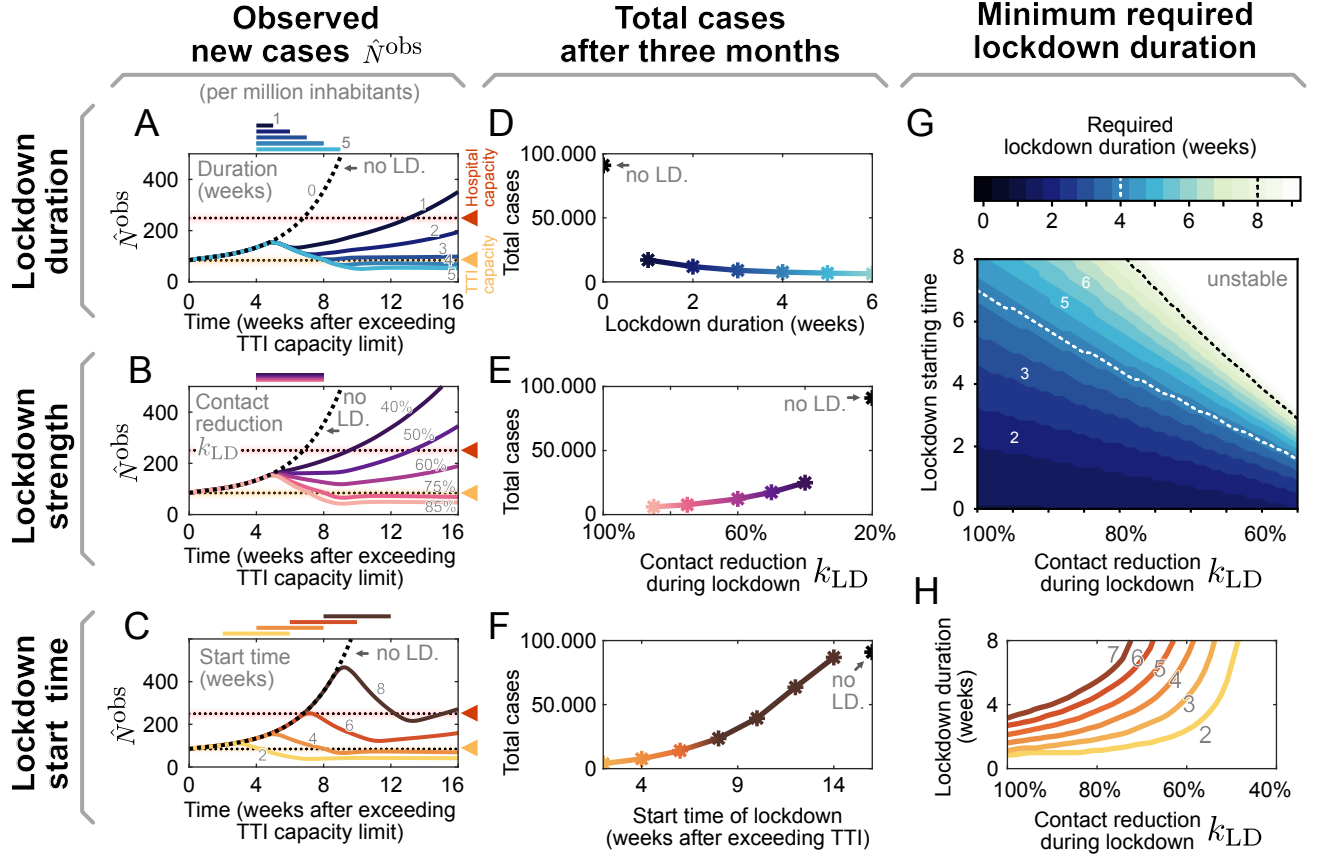


Figure 4: **The effectiveness of a lockdown depends on three main parameters: its duration, strength and starting time.** (A–C) Observed daily new cases for a lockdown (abbreviated as LD in the figure) that is enacted after the TTI capacity has been exceeded. Reference parameters are a lockdown duration of 4 weeks, contact reduction during lockdown of $k_{LD} = 75\%$ and a start time at 4 weeks after exceeding TTI capacity. (A) Lockdown duration: between 0 weeks (no lockdown) to 5 weeks. Case numbers are lowered below TTI capacity after a minimum of 4 weeks for default lockdown settings. (B) Lockdown strength: Lockdown strengths can be measured by the amount of contact reduction during the lockdown k_{LD} . The stronger a lockdown, the shorter is the duration that is required to push daily case numbers below the TTI capacity. (C) Lockdown starting time. The start time is given in weeks after the TTI capacity was exceeded. The sooner a lockdown is enacted, the more effective it can be: For late start times (≥ 6 weeks), case numbers cannot be brought below TTI capacity with the reference lockdown of 4 weeks. (D–F) Total cases after three months, if the lockdown is parameterized as described in panels A–C, respectively. (G, H) **Lockdown duration, strength and start time are complementary:** How does the minimum lockdown duration that is required to reduce case numbers below TTI capacity depend on the starting time and the contact reduction during the lockdown? (G) Lower left, dark region: Heavy contact reduction and timely lockdown enacting can make even short lockdowns (≤ 2 weeks) effective. Upper right, bright region: Moderate contact reduction and late start times require increasingly long lockdowns. For mild contact reduction and very late start times, lockdowns become ineffective even when they last indefinitely — the system is unstable and case numbers increase. (H) Horizontal slices through the colormap (G). Here, colors match panels (C, F) and correspond to the lockdown start time.

insufficient lockdown, the faster case numbers will rise again. Also, it might be advantageous to not stop right below the TTI limit, but to establish a safety-margin for robustness. Overall, the major challenge is not to ease the lockdown too early, as otherwise the earlier success is soon squandered.

When a lockdown is implemented, it is necessary to reduce contagious contacts k_t severely in order to decrease case numbers below the TTI capacity limit (Fig. 4 B). In our model scenario, the contacts have to be reduced by at least $k_{LD} = 75\%$ to bring the system back to a stable regime. A lockdown that is only slightly weaker cannot reverse the spread to a decline of cases (even if $k_{LD} > k_t^{\text{crit}} \approx 60\%$, Fig. 4 B). Furthermore, increasing

the lockdown strength decreases the required lockdown duration (Fig. 4 G and H). This shows that stricter lockdowns imply shorter-lasting social and economical restrictions.

The earlier a lockdown begins after exceeding the TTI capacity limit, the faster control can be re-established and constraints can be loosened again (Fig. 4 C). If started right after crossing the threshold, in principle, only a few days of lockdown are necessary to bring back case numbers below TTI capacity limit. On the other hand, if only starting four or six weeks later, the lockdown duration necessary to reach the stable regime becomes increasingly long and leads to a significantly larger amount of total cases (Fig. 4 F) and fatalities.

Interestingly, either a lockdown is strong enough to reach control within a few weeks – or else it fails to do so almost completely (Fig. 4 G). The parameter regime between these two options is quite narrow, thus it is not very likely to be realized over long weeks. For practical policies this means that — if a lockdown does not start to show clear effect after 2 or 3 weeks, should revise the strategy.

2.6 Long-term perspective: Repeated lockdowns are not required to maintain control over the COVID-19 spread

A natural goal would be to keep case numbers below the hospital capacity. However, our model suggests that keeping them below TTI capacity requires less contact restrictions, less lockdown duration, and costs less lives. In the following we compare these two goal — keep case numbers either below TTI capacity or below hospital capacity. We assume that with crossing the respective capacity limit a circuit breaker is enacted. Here, we study the long-term perspective of these two circuit-breaker strategies and their dependence on the contact reduction when not in lockdown.

To study the relative contribution of the different factors involved in the circuit-breaker dynamics (Fig. 5), we start from an unstable condition, where the base contact reduction $k_0 = 20\%$ is not sufficient to control the spread, and we enact a two-week lockdown when crossing either the TTI or the hospital capacity. During the lockdown, contacts are reduced by $k_{LD} = 75\%$. After the first and all subsequent lockdowns, contacts k_{nLD} are reduced by 20%, 40% or 60% relative to pre-COVID levels, thus mildly, moderately, or strongly.

Assuming mild contact reduction after lockdowns ($k_{nLD} = 20\%$), then case numbers rise after lifting the lockdown, independent of the chosen threshold (TTI or Hospital capacity, Fig. 5 A). In both scenario, repeated regulatory lockdowns are necessary to prevent the health care system from being overwhelmed. In contrast, if the contact reduction after the first lockdown remains relatively strong ($k_{nLD} = 60\%$, Fig. 5 C), then case numbers are stabilized and no further lockdowns are required.

Interestingly, maintaining moderate contact reduction while not in lockdown ($k_{nLD} = 40\%$, Fig. 5 B), is sufficient to stay within the metastable regime of low case numbers (as long as TTI is not overwhelmed). This opens a promising perspective for a mid- or long-term control strategy: Once case numbers are below the TTI limit (after an initial lockdown), maintaining a moderate reduction of contacts is sufficient to enable a long-term control of the spread, without additional lockdowns (Fig. 5 B, yellow line). However, if case numbers are only below hospital capacity but above TTI capacity limit, the same, moderate contact reduction requires repeated lockdowns (Fig. 5 B, red line).

The advantage of the strategy to stay below the TTI capacity limit becomes very clear when considering the total cost of the required lockdowns: Independently of the level of contact reduction, (i) the total number of cases (and consequently deaths and long-COVID risk) is lower (Fig. 5 D), (ii) the total duration spent in lockdown is shorter (Fig. 5 E), and (iii) the frequency at which lockdowns have to reoccur is lower (Fig. 5 A). As case numbers and lockdown duration indicate economic costs, a strategy that respects the TTI limit offers a low economic toll, enables mid-term planning and provides trust to people and society.

In future, large-scale testing and immunization certainly will play a role for long-term strategies. The availability of cheap, fast, and reliable tests will make large-scale random testing possible and facilitate the early detection of infection chains, as it improves the efficiency of TTI [26–29] (Fig. 5 F). However, for random testing to show effect, a large number of individuals has to be tested. For instance, a naive random testing rate λ_r of 5% would lower to necessary contact reduction below 10%, but would require every individual to be tested every 20 days. When larger fractions of the population are immunized (either through vaccination or lasting post-infection immunity), the minimum required reduction of contacts becomes lower. These are signs of saturation towards herd immunity (Fig. 5 G, see Supplementary Section 4 for further discussion).

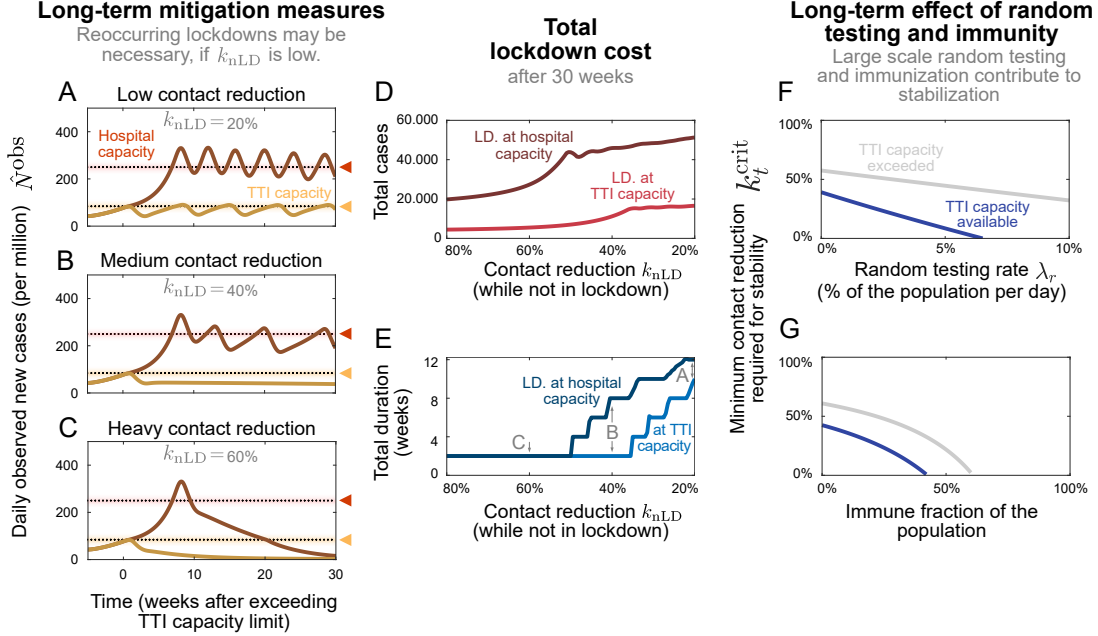


Figure 5: **On a long-term perspective, lockdowns are not required repeatedly if the subsequent contact reduction k_{nLD} is sufficient to keep case numbers constant.** When case numbers are low, fewer lockdowns (abbreviated as LD in the figure) are required than at high case numbers. (A–C) Daily observed new cases per million for different levels of sustained contact reduction k_{nLD} , which is maintained after the lockdowns. We assume that a two-week lockdown is either enacted when the TTI capacity limit is crossed (yellow lines), or when the hospital capacity limit is crossed (red lines), and that the effective contact reduction takes one week to ramp from its value in non-lockdown to the lockdown situation ($k_{nLD} \rightarrow k_{LD}$). (A) Given only a mild contact reduction $k_{nLD} = 20\%$ when no lockdown is imposed, lockdowns need to reoccur with a high frequency, which gets even higher when TTI is overwhelmed and case numbers are near hospital capacity. (B) For a moderate contact reduction $k_{nLD} = 40\%$, lockdowns only need to reoccur if they fail bringing case numbers within TTI capacity where case numbers can be controlled illustrated by the short lockdowns enacted after crossing hospital capacity (red curve). (C) For heavy contact reduction $k_{nLD} = 60\%$, lockdowns do not need to reoccur, even when enacted only at high case numbers. (D, E) The total cost (in terms of cumulative cases and total lockdown duration) depends on the level of contact reduction and the lockdown policy: It is lower when lockdowns are initiated at the TTI capacity limit and when contact reduction k_{nLD} in between lockdowns is high. (F, G) In the future, the required contact reduction for marginal stability k_t^{crit} may be lowered by the implementation of large-scale random testing (F) or by immunization of the population (G).

3 Discussion

We demonstrated that between the two extremes of eradication and high case numbers close to or beyond the hospital capacity limit, stable and metastable regimes of SARS-CoV2 spreading exist. In such regimes, every person only has to reduce their contacts moderately, while case numbers still can be maintained robustly at low levels. The contact reduction can be milder if case numbers are sufficiently low, so that the test-trace-isolate (TTI) system can act efficiently and quickly to break infection chains. We explored how these regimes can be regained through lockdowns after TTI systems have been overwhelmed, and we showed long-term perspectives given different mitigation strategies.

To focus on the general spreading dynamics, we made several simplifying assumptions. First, we assumed that spreading happens homogeneously in the population, without regional differences. With this simplification, our model predicts the level, at which case numbers reach the national TTI capacity, but due to heterogeneities of the spread and TTI capacity, regional TTI limits can be reached earlier than what nationwide case numbers imply. Second, we did not consider age-related transmission, contact and incidence differences, which could lead to similar effects. Third, we assumed in our scenarios that the behavior of the population and subsequent contact reduction is constant over time (except during lockdown). Real situations are more dynamic, necessitating frequent reevaluations of the current restrictions and mitigation measures. The effect of inhomogeneous populations may have a similar effect like simulating distinct, but coupled populations,

or, like simulating one population that is subject to some external input Φ_t . Hence, varying the input Φ_t can — to a first approximation — serve to explore coupled, inhomogeneous populations. For our results that would imply that inhomogeneity — like Φ_t — changes the absolute values of the equilibrium, and might even destabilize it.

Quantitatively, our assumptions regarding the efficiency of TTI are in agreement with those of other modeling studies. Both agent-based studies with detailed contact structures [30, 31] as well as studies using mean-field spreading dynamics [32–36] agree that TTI measures are an important contribution to control the pandemic, but success depends strongly on how well they are implemented. For an efficient TTI implementation, fast testing, rigorous isolation, and a large fraction of traced contacts are essential [30, 31]. Given our informed assumptions about these parameters, our model shows that TTI only can compensate for a basic reproduction number R_0 of 3.3 — if in addition contagious contacts are reduced by about 40 % (95% CI: [24, 53] %). This is comparable to the results of other studies [30, 31, 33, 37, 38].

In the following we put our modeling results into perspective with respect to the dynamics of COVID-19 observed in Germany and Europe (for an extended discussion of several countries throughout the world see Supplementary Notes, Section S2.1). We then discuss the impact of the central factors, and finally stress again the importance of behavior for contact reduction.

3.1 Recent COVID-19 spreading dynamics in Europe may reflect exceeded TTI capacity

Indications of a transition from the TTI stabilized regime to a regime of self-accelerated spread can be found in various countries. In our model, the self-acceleration of the spread does not unfold instantaneously but throughout four to eight weeks after crossing the TTI limit (cf. Fig. 3). Various countries, especially in Europe, have shown a rapid increase in case numbers, that sets in after exceeding around 20 to 50 daily new cases per million. For example, a Bayesian inference analysis of German case numbers finds a substantial increase of the effective daily growth rate that lasted for around 4 weeks throughout October (Fig. 6, [39]). Other European countries showed comparable dynamics, but at different times (Fig. S4). Many of these countries transitioned from a nearly stabilized state to an uncontrolled spread — in qualitatively similar ways that may be related to exceeding TTI capacity.

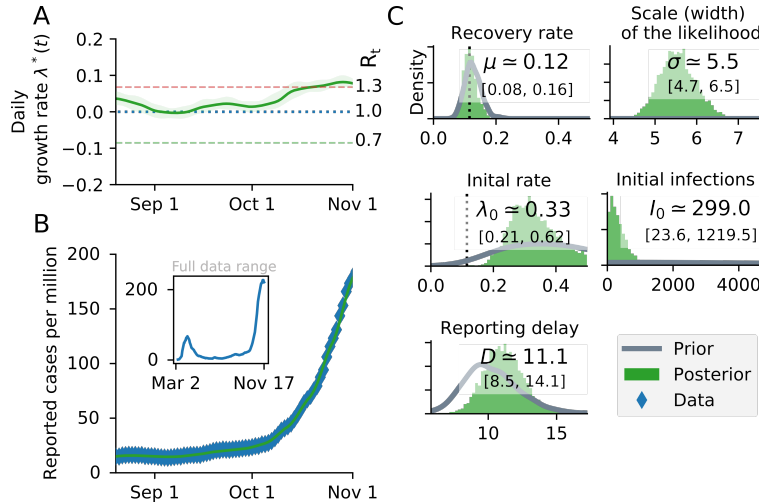


Figure 6: **A substantial increase in the effective growth rate in Germany occurred during the month of October, suggesting that regional TTI capacity limits were exceeded.** (A) Before October, the reproduction number was slightly above one (corresponding to a daily growth rate λ^* slightly above zero). (B) Observed case numbers were stabilized below 20 daily new cases per million (but still, slowly growing), until a transition into the unstable regime took place over ~ 4 weeks in October. The time range is adjusted to focus on this tipping point. The inset shows case numbers for the full available time range. (C) Main central epidemiological parameters with prior and posterior distribution.

3.2 Strategies to face COVID-19 differ among countries

Strategies to face COVID-19 differ among countries and are reflected in the case numbers. Very low case numbers and even local eradication has been achieved by several South- and East-Asian countries, Australia

and New-Zealand. By aiming for local eradication, these countries reached very low case numbers (below one daily new case per million, Supp. Fig. S2 C). If local eradication is successful, these countries can profit from the absorbing state of zero SARS-CoV-2 infections.

In many European countries over the summer, case numbers were relatively low, typically around 10 daily new cases per million (Fig. S2 B) and contacts were only mildly restricted. However, at the end of summer, many countries suffered a second wave (Supp. Fig. S4) that cannot be explained by seasonality alone (cf. Supp. Sec. S2.1). In Europe, it would be difficult to reach the extremely low levels of about one daily new case per million because an external influx from neighboring countries cannot be prevented. Nonetheless, the stabilized case numbers in Europe during summer show that this regime can be maintained.

Sustained high levels of more than 100 daily new cases per million have been observed in several (but not all and not exclusively) American countries (Supp. Fig. S2 A). This shows that high levels of daily new infections can be maintained in principle. However, the stringency of interventions is similar to other countries (see [40]), and the prospect of reaching herd immunity is still far away.

In our results on long-term strategies that focused on a 30 week time frame, first signs of herd immunity could be observed at high case numbers (Fig. 5 B): At high case numbers, the need for regulatory lockdowns became less frequent over time. However, the cost of aiming for herd immunity in a real-world scenario, is a high number of infected, hospitalized, and deceased people, besides those recovered individuals who potentially will suffer from “long COVID” [2–5, 41], the concurrent high risk for anyone to get infected, as well as long-term burden to the health care system. Stability through herd immunity is only possible if the post-infection immunity lasts for years, which is unclear as of yet [1, 42–45]. Nonetheless, this phenomenon shows that immunity effects play an increasing role as model predictions extend further into the future — and dedicated modeling is required to address immunity properly.

3.3 Central parameters of our model

To be effective, TTI implementations must provide sufficient test capacity, and tracing should be fast and extensive. If implemented with parameters similar to German or European systems during summer, then according to our model only about 40% instead of 60% reduction are necessary to stabilize the spread. In other words, if case numbers are low, all the available test and trace efforts can be concentrated on the remaining infection chains and thereby increase their effectiveness in mitigation. We did not model this effect explicitly, but it would further facilitate a control at low case numbers and in fact such a trend had been observed during spring in Germany.

We assumed that TTI reaches its capacity limit at about 100 daily new infected per million. This value is comparably high, but still within the range that could be traced in Germany with considerable effort. The precise limit of contact tracing depends on a number of factors, including the personnel at the tracing units, potentially a tracing app [33], and the number of relevant contacts a person has on average. Already the latter factor can easily differ by a factor 10, depending on contact restrictions. However, for the qualitative dynamics, the precise value of the tracing capacity does not matter too much (as long as it is high enough or as long as case numbers are low): As long as the system is (meta-) stable, the equilibrium value of new infected is determined by Φ_t and k_t , and is typically far below this TTI limit, typically well below 10 daily new cases per million (Fig. 2). Thus, stable systems either tend to equilibrate far below the TTI limit, or else they are very close to tipping over (Fig. 2A, Fig. 3E). The TTI limit plays a central role in informing policymakers when to issue preventive measures: if approaching that limit, the risk of tipping over to uncontrolled spread strongly increases, and countermeasures then should be taken early. Otherwise, the spread might self-accelerate and get out of control.

3.4 Conclusion and Outlook

Our results show that a stable equilibrium regime at low case numbers exists and can be maintained with a moderate contact reduction (about 40% less contagious contacts compared to pre-COVID-19). In that regime, a certain level of new imported infections (Φ_t) can be compensated and no further lockdowns or circuit breakers are necessary.

A moderate reduction of infectious contacts k_t of 40 to 60% can be achieved with preventive mitigation measures, as shown by studies analyzing the effectiveness of non-pharmaceutical interventions during the first wave [39, 46–48]. Restrictions on the maximum size of gatherings to 100 people already lead to effective reductions in the range of 10 to 40% [39, 46, 48]. Improved hygiene, frequent ventilation of rooms, and the compulsory use of masks can further reduce the number of infectious contacts, yet, by a factor that is

more difficult to estimate [49–51]. When the aim is to stay in the metastable regime of low case numbers below TTI capacity, then only a moderate contact reduction is required to stabilize the system; reoccurring lockdowns are not necessary. Hence, this regime is very promising for a mid- and long-term management of the pandemic, until a vaccination or better treatment of COVID is developed, as it poses the least burden on economy and society.

The alternative option is to stabilize case numbers at higher levels (below the hospital capacity), which requires a stronger contact reduction (about 60%). This is because testing and tracing become less efficient. However, if case numbers are stabilized at the high level and then need to be lowered, an even stronger contact reduction of 75% over the duration of a lockdown (a few weeks) is necessary to achieve a suppression of the spread. From the past studies on the effectiveness of interventions, it seems unlikely that such a reduction can be achieved without incisive measures, including potentially the closure of schools and public businesses, stay-at-home orders, and contact bans [39, 46, 47]. This assessment is in line with the experience of e.g. Israel and Ireland during the second wave. Thus, stabilizing the spread at higher levels of case numbers counterintuitively requires more stringent (and repeated) measures than a stabilization at low case numbers.

Concluding, the recommendation from this paper is to achieve and maintain low case numbers that ensure an efficient operation of TTI measures. To maintain this regime, one needs to counteract local super-spreading events or extensive influx of new cases as early as possible. If throughout Europe, or even internationally, low case numbers are reached and maintained, then every country profits from the stability of their neighbors.

References of main text and supplementary

The supplementary references will be moved to supplementary file in the final submission (from Ref. 52 onwards).

- [1] N. A. Alwan, *et al.*, *The Lancet* **6736**, 19 (2020).
- [2] E. Fraser, *BMJ* **370** (2020).
- [3] R. Rubin, *JAMA* **324**, 1381 (2020).
- [4] T. Greenhalgh, M. Knight, C. A’Court, M. Buxton, L. Husain, *BMJ* **370** (2020).
- [5] E. J. Topol, *Science* **370**, 408 (2020).
- [6] A. Scherbina, *Economics Working Paper* **3** (2020).
- [7] Z. Lin, C. M. Meissner, *Public Health Policies and the Economy During Covid-19 (May 2020)*. NBER Working Paper (2020).
- [8] R. Li, *et al.*, *Science* **368**, 489 (2020).
- [9] W. O. Kermack, A. G. McKendrick, *Proceedings of the royal society of london. Series A, Containing papers of a mathematical and physical character* **115**, 700 (1927).
- [10] H. W. Hethcote, *Theoretical population biology* **14**, 338 (1978).
- [11] H. W. Hethcote, *SIAM Review* **42**, 599 (2000).
- [12] S. Contreras, *et al.*, *arXiv preprint arXiv:2009.05732* (2020).
- [13] C.-C. Lai, *et al.*, *Journal of Microbiology, Immunology and Infection* (2020).
- [14] Y. Liu, A. A. Gayle, A. Wilder-Smith, J. Rocklöv, *Journal of travel medicine* (2020).
- [15] O. Byambasuren, *et al.*, *Available at SSRN 3586675* (2020).
- [16] M. Pollán, *et al.*, *The Lancet* (2020).
- [17] J. H. McDermott, W. G. Newman, *Clinical Medicine* (2020).
- [18] S. Zhao, *et al.*, *International Journal of Infectious Diseases* **92**, 214 (2020).
- [19] Y. Alimohamadi, *et al.*, *J Prev Med Public Health* **53**, 151 (2020).
- [20] A. Barber, *et al.*, *medRxiv* (2020).
- [21] J. P. La Salle, *The stability of dynamical systems* (SIAM, 1976).
- [22] J. Wilting, V. Priesemann, *Nature Communications* **9**, 2325 (2018).
- [23] M. J. Keeling, *et al.*, *medRxiv* p. 2020.10.13.20211813 (2020).
- [24] E. Mahase, *BMJ* **371** (2020).
- [25] Z. Kmietowicz, *BMJ* **371** (2020).

- [26] E. Holt, *The Lancet* **396**, 1386 (2020).
- [27] M. J. Mina, R. Parker, D. B. Larremore, *New England Journal of Medicine* **0**, null (2020).
- [28] D. B. Larremore, *et al.*, *medRxiv* (2020).
- [29] N. Kumleben, *et al.*, *Public Health* **185**, 88 (2020).
- [30] A. J. Kucharski, *et al.*, *The Lancet Infectious Diseases* **0** (2020).
- [31] C. C. Kerr, *et al.*, *medRxiv* p. 2020.07.15.20154765 (2020).
- [32] C. Fraser, S. Riley, R. M. Anderson, N. M. Ferguson, *Proceedings of the National Academy of Sciences* **101**, 6146 (2004).
- [33] L. Ferretti, *et al.*, *Science* **368** (2020).
- [34] D. Lunz, G. Batt, J. Ruess, *medRxiv* p. 2020.05.26.20113340 (2020).
- [35] S. Sturniolo, W. Waites, T. Colbourn, D. Manheim, J. Panovska-Griffiths, *medRxiv* (2020).
- [36] T. Colbourn, *et al.*, *SSRN Electronic Journal* pp. 1–80 (2020).
- [37] J. Hellewell, *et al.*, *The Lancet Global Health* (2020).
- [38] E. L. Davis, *et al.*, *medRxiv* (2020).
- [39] J. Dehning, *et al.*, *Science* (2020).
- [40] T. Hale, S. Webster, A. Petherick, T. Phillips, B. Kira, Oxford COVID-19 Government Response Tracker, Blavatnik School of Government. , <https://www.fda.gov/media/136472/download> (2020).
- [41] *Nature* **586**, 170 (2020).
- [42] Y. Chen, *et al.*, *PLOS Pathogens* **16**, e1008796 (2020).
- [43] T. J. Ripperger, *et al.*, *Immunity* **53**, 925 (2020).
- [44] N. Kaneko, *et al.*, *Cell* **183**, 143 (2020).
- [45] A. W. D. Edridge, *et al.*, *Nature Medicine* **26**, 1691 (2020).
- [46] J. M. Brauner, *et al.*, *medRxiv* (2020).
- [47] S. Hsiang, *et al.*, *Nature* **584**, 262 (2020).
- [48] Y. Li, *et al.*, *The Lancet Infectious Diseases* (2020).
- [49] D. K. Chu, *et al.*, *The Lancet* **395**, 1973 (2020).
- [50] J. Howard, *et al.* (2020).
- [51] L. Morawska, *et al.*, *Environment International* **142**, 105832 (2020).
- [52] E. O.-O. Max Roser, Hannah Ritchie, J. Hasell, *Our World in Data* (2020). <https://ourworldindata.org/coronavirus>, (Europe, America, and Oceania and Asia).
- [53] A. Kronbichler, *et al.*, *International Journal of Infectious Diseases* (2020).
- [54] L. Huang, *et al.*, *Journal of Infection* (2020).
- [55] E. Lavezzo, *et al.*, *Nature* (2020).
- [56] N. V. V. Chau, *et al.*, *Clinical Infectious Diseases* (2020).
- [57] M. Cevik, K. Kuppalli, J. Kindrachuk, M. Peiris, *BMJ* **371** (2020).
- [58] J. A. Firth, *et al.*, *medRxiv* (2020).
- [59] S. Kojaku, L. Hébert-Dufresne, Y.-Y. Ahn, *arXiv preprint arXiv:2005.02362* (2020).
- [60] M. an der Heiden, O. Hamouda, *Epidemiologisches Bulletin* **2020**, 10 (2020).
- [61] S. A. Lauer, *et al.*, *Annals of internal medicine* (2020).
- [62] L. F. Shampine, S. Thompson, *Applied Numerical Mathematics* **37**, 441 (2001).
- [63] E. Jarlebring, *The delay e-letter* **2**, 155 (2008).
- [64] L. N. Trefethen, *Spectral methods in MATLAB* (SIAM, 2000).
- [65] X. He, *et al.*, *Nature Medicine* pp. 1–4 (2020).
- [66] F. Pan, *et al.*, *Radiology* p. 200370 (2020).
- [67] Y. Ling, *et al.*, *Chinese medical journal* (2020).

- [68] Y. M. Bar-On, A. Flamholz, R. Phillips, R. Milo, *Elife* **9**, e57309 (2020).
- [69] A. F. Siegenfeld, Y. Bar-Yam, *Communications Physics* **3**, 204 (2020).
- [70] P. Bittihn, R. Golestanian, *arXiv:2003.08784 [physics, q-bio]* (2020). ArXiv: 2003.08784.
- [71] M. Linden, *et al.* pp. 1–7 (2020).
- [72] A. T. Levin, *et al.*, *medRxiv* (2020). MedRxiv: 10.1101/2020.07.23.20160895v5.
- [73] Great Barrington declaration and petition, <https://gbdeclaration.org/> (2020).
- [74] R. S. Bhopal, *Public Health in Practice* **1**, 100031 (2020).
- [75] J. Salvatier, T. V. Wiecki, C. Fonnesbeck, *PeerJ Computer Science* **2**, e55 (2016).

Author Contributions

S.C, J.D., and V.P. designed the research. S.C., J.D., S.M., and P.S. conducted the research. All authors analyzed the data. S.C., S.M., and P.S. created the figures. All authors wrote the paper.

Competing Interests

The authors declare no competing interests.

Data availability

Both data [52] and analysis code https://github.com/Priesemann-Group/covid19_research/tree/master/circuit_breaker are available online. Additionally, an interactive platform to simulate scenarios different from those presented here will be soon available (beta-version). The permanent link will be provided in the same GitHub repository.

Acknowledgments

We thank Melanie Brinkmann and Álvaro Olivera-Nappa for their helpful comments and encouraging feedback. We thank M. Loidolt, Michael Wibrál and Johannes Zierenberg from our group for carefully reading, commenting and improving the manuscript. We thank the Priesemann group for exciting discussions and for their valuable input. **Funding:** All authors received support from the Max-Planck-Society. JD and PS acknowledge funding by SMARTSTART, the joint training program in computational neuroscience by the VolkswagenStiftung and the Bernstein Network.

S1 Methods

Model overview. We model the spreading dynamics of SARS-CoV-2 as the sum of contributions from two pools of infectious individuals, i.e. quarantined-isolated I^Q and hidden non-isolated I^H individuals, while also modeling the infectivity timeline through the incorporation of compartments for individuals exposed to the virus (E^Q , E^H), following an SEIR-like formalism. The quarantined infectious pool (I^Q) contains cases revealed through testing or by contact tracing and subsequently sent to quarantine-isolation and avoid further contacts as well as possible. In contrast, in the hidden infectious pool (I^H), infections spread silently and only become detectable when individuals develop symptoms and get tested, via random testing in the population or as part of the chain of contacts of recently identified individuals. This second pool (I^H) is called the hidden pool; individuals in this pool are assumed to exhibit the general population’s behavior, thus of everyone who is not aware of being infected. Healthy individuals that can be infected belong to the susceptible pool S , while we assume that, after they recover and for the relatively short time-frame here studied, they remain immunized in the R compartment. For a graphical representation of the model, the reader is referred to Supplementary Fig. S1. We model the mean-field interactions between compartments by transition rates, determining the timescales involved. These transition rates can implicitly incorporate both the time course of the disease and the delays inherent to the TTI process. Individuals exposed to the virus become infectious after the latent period, modeled by the We distinguish between symptomatic and asymptomatic carriers – this is central when exploring different testing strategies (as detailed below). We also include the effects of non-compliance, modeled as a higher asymptomatic ratio, and imperfect contact tracing, including an explicit delay between testing and tracing of contacts. In the different scenarios analyzed, we include a non-zero influx Φ_t of new cases that acquired the virus from outside. Even though this influx makes a complete eradication of SARS-CoV-2 impossible, different outcomes in the spreading dynamics might arise depending on both contact intensity and TTI. We then investigate the system’s stability and dynamics, aiming to control the spread with a low total number of cases without necessitating a too large reduction of infectious contacts.

S1.1 Spreading Dynamics

Concretely, we use a modified SEIR-type model, where infected individuals can be either symptomatic or asymptomatic. They belong to hidden (E^H , I^H) or a quarantined (E^Q , I^Q) pools of infections, thus creating in total one compartment of susceptible (S), two compartments of exposed individuals (E^H , E^Q), four compartments of infectious individuals ($I^{H,s}$, $I^{H,a}$, $I^{Q,s}$, $I^{Q,a}$), and one compartment for recovered/removed individuals (R).

New infections are asymptomatic with a ratio ξ , the others are symptomatic. In all compartments individuals are removed with a rate γ because of recovery or death (Supplementary Table S1 for all parameters).

In the hidden pools, the disease spreads according to the contact patterns of the population, which can be expressed as a fraction k_t of the intensity they had before COVID-19 related contact-restrictions. Defining R_0 as the base reproduction number without contact restrictions, the reproduction number of the hidden pool I^H is given by $(1 - k_t) R_0$. This reproduction number reflects the disease spread in the general population, without testing induced isolation of individuals. Additionally, the hidden pool receives a mobility-induced influx Φ_t of new infections. Cases are removed from the hidden pool (i) when detected by TTI and put into the quarantined pool I^Q , or (ii) due to recovery or death.

The quarantined exposed and infectious pools (E^Q , I^Q) contain those infected individuals who have been tested positive as well as their positively tested contacts. Infectious individuals in I^Q are (imperfectly) isolated, we assume their contacts have been reduced to a fraction $(\nu + \epsilon)$ of the ones they had in pre-COVID-19 times, of which only ν are captured by the tracing efforts of the health authorities, and the subsequent infections remain quarantined, thus entering the E^Q pool and afterwards the I^Q pool. The remaining fraction of produced infections, ϵ , are missed and act as an influx to the hidden pools (E^H). Therefore, the overall reproduction number in the I^Q pool is $(\nu + \epsilon) R_0$.

As our model is an expanded SEIR-model, it assumes post-infection immunity, which is a realistic assumption given the limited time-frames considered in our analysis. Our model can also reflect innate immunity; one then has to rescale the population or the reproduction number. The qualitative behavior of the dynamics is not expected to change.

S1.2 Parameter Choices and Scenarios

For any testing strategy, the fraction of infections that do not develop any symptoms across the whole infection timeline is an important parameter, and this also holds for testing strategies applied to the case of SARS-CoV-2. In our model this parameter is called ξ^{ap} and includes beside true asymptomatic infections ξ also the effect of individuals that avoid testing [17]. The exact value of the fraction of asymptomatic infections ξ , however, is still fraught with uncertainty, and it also depends on age [13, 53, 54]. While early estimates were as high as 50% (for example ranging from 26% to 63% [55]), these early estimates suffered from reporting bias, small sample sizes and sometimes included pre-symptomatic cases as well [15, 56]. Recent studies estimate the asymptomatic transmission to be more minor [57], estimates of the fraction of asymptomatic carriers range between 12% [15] and 33% [16].

Another crucial parameter for any TTI strategy is the reproduction number of the hidden infections. This parameter is by definition impossible to measure, but it presents typically the main driver of the spreading dynamics. It depends mainly on the contact behavior of the population, and ranges from R_0 in the absence of contact restrictions to values below 1 during strict lockdown [39]. Herein we decided to include instead the reduction of contacts with respect to the pre-COVID-19 base-line k_t to represent the reproduction number of hidden infections I^H , which would be proportional to $(1 - k_t)R_0$. For the default parameters of our model, we evaluated different levels of contact reduction k_t .

S1.3 Testing-and-Tracing strategies

We consider a testing-and-tracing strategy: symptom-driven testing and specific testing of traced contacts, with a subsequent of the cases tested positive. Our model can also include random testing, but this case is not explored in the scenarios of this paper.

Symptom-driven testing is defined as applying tests to individuals presenting symptoms of COVID-19. In this context, it is important to note that non-infected individuals can have symptoms similar to those of COVID-19, as many symptoms are rather unspecific. Although symptom-driven testing suffers less from imperfect specificity, it can only uncover symptomatic cases that are willing to be tested (see below). Here, *symptomatic, infectious individuals* are transferred from the hidden to the traced pool at rate λ_s .

We define λ_s as the daily rate at which symptomatic individuals get tested, among the subset who are willing to get tested, because of surveillance programs or self-report. As default value we use $\lambda_s = 0.25$, which means that, on average, an individual willing to get tested that develops COVID-19-specific symptoms would get a test within 4 days from the end of latency. Testing and isolation happens immediately in this model, but their report into the observed new daily cases \hat{N}^{obs} is delayed, and so is the tracing of their contacts.

Tracing contacts of positively tested infectious individuals presents a very specific test strategy, and is expected to be effective in breaking the infection chains, if contacts self-isolate sufficiently quickly [30, 58, 59]. However as every implementation of a TTI strategy is bound to be imperfect, we assume that only a fraction $\eta < 1$ of all contacts can be traced. These contacts, if tested positive, are then transferred from the hidden to the quarantined infectious pools ($I^H \rightarrow I^Q$) with an average delay of $\tau = 2$ days. The parameter η effectively represents the fraction of secondary and tertiary infections that are found through contact-tracing. As this fraction decreases when the delay between testing and contact-tracing increases we assumed a default value of $\eta = 0.66$, i.e. on average only two thirds of subsequent offspring infections are prevented. Contact tracing is mainly done by the health authorities in Germany, and this clearly limits the maximum number $N_{\text{max}}^{\text{test}}$ of new cases observed through testing N^{test} , for which contact tracing is still functional.

Random testing is defined here as applying tests to individuals irrespective of their symptom status, or whether they belonging to the contact-chain of other infected individuals. In our model, random testing transfers infected individuals from the hidden to the quarantined infectious pools with fixed rate λ_r , irrespective of them showing symptoms or not. In reality, random testing is often implemented as situation-based testing for a sub-group of the population, e.g. at a hot-spot, for groups at risk, or for people returning from travel. Such situation-based strategies would be more efficient than the random testing assumed in this model, which may be unfeasible in a country level due to testing limitations [12].

S1.4 Lockdown modelling

To assess the effectiveness of lockdowns in the broad spectrum of contact-ban governmental interventions, we model how the reduction of contacts and the duration of such restrictive regimes help lower case numbers.

We model contact reductions as reductions in the reproduction number of the hidden population, which for these matters is presented as percentages of the basic reproduction number R_0 , which sets the pre-COVID-19 base-line for the number of close contacts.

For the sake of simplicity, we assume the lockdown has three signature stages: i) uncontrolled regime, where the TTI capacity is overwhelmed because of high case numbers and unsustainable contact intensity, reflected by a high value of $k_t = k_0$ and high influx of infections Φ_t . ii) Strong reduction of contacts $k_0 \rightarrow k_{LD}$ and borders closing $\Phi_t \rightarrow \Phi_{LD}$. iii) Relaxation of measures to a new level, where the system should be again stable, within the TTI-based stability $k_{LD} \rightarrow k_{nLD}$, and borders would be open $\Phi_{LD} \rightarrow \Phi_{nLD}$. All the changes between the different regimes i \rightarrow ii \rightarrow iii are modelled as linear ramps for both parameters, which take D_{ramp} days to reach their set-point. The duration of the lockdown D_L , namely, the time-frame between the start of the restrictive measures and the beginning of their relaxation, is measured in weeks, and its default length – for analysis purposes – is four weeks.

S1.5 Model Equations

The contributions of the spreading dynamics and the TTI strategies are summarized in the equations below. They govern the spreading dynamics of case numbers in and between the different susceptible-exposed-infectious-recovered (SEIR) pools, both hidden -non-isolated- and quarantined -under surveillance-. We assume a regime where most of the population is susceptible, and the time-frame analyzed is short enough to assume post-infection immunity. Thus, the dynamics are completely determined by spread (characterized by the reproduction numbers $(1 - k_t) R_0$, $(\nu + \epsilon) R_0$), transition from exposed to infectious (at rate ρ), recovery (characterized by the recovery rate γ), external influx Φ_t and the impact of the TTI strategies:

$$\frac{dS}{dt} = - \underbrace{\gamma(1 - k_t) R_0 \frac{S}{M} I^H}_{\text{hidden contagion}} - \underbrace{\gamma(\nu + \epsilon) R_0 \frac{S}{M} I^Q}_{\text{traced contagion}} - \underbrace{\frac{S}{M} \Phi_t}_{\text{ext. influx}}, \quad (1)$$

$$\frac{dE^Q}{dt} = \underbrace{\gamma \nu R_0 \frac{S}{M} I^Q}_{\text{traced contagion}} + \underbrace{\chi_\tau N^{\text{traced}}}_{\text{contact tracing}} - \underbrace{\rho E^Q}_{\text{end of latency}}, \quad (2)$$

$$\frac{dE^H}{dt} = \underbrace{\gamma \frac{S}{M} ((1 - k_t) R_0 I^H + \epsilon R_0 I^Q)}_{\text{hidden contagion}} - \underbrace{\chi_\tau N^{\text{traced}}}_{\text{contact tracing}} - \underbrace{\rho E^H}_{\text{end of latency}}, \quad (3)$$

$$\frac{dI^Q}{dt} = \underbrace{\rho E^Q - \gamma I^Q}_{\text{spreading dynamics}} + \underbrace{N^{\text{test}}}_{\text{testing}} + \underbrace{(\chi_{s,r}(1 - \xi) + \chi_r \xi) N^{\text{traced}}}_{\text{contact tracing}}, \quad (4)$$

$$\frac{dI^H}{dt} = \underbrace{\rho E^H - \gamma I^H}_{\text{spreading dynamics}} - \underbrace{N^{\text{test}}}_{\text{testing}} - \underbrace{(\chi_{s,r}(1 - \xi) + \chi_r \xi) N^{\text{traced}}}_{\text{contact tracing}} + \underbrace{\frac{S}{M} \Phi_t}_{\text{ext. influx}}, \quad (5)$$

$$\frac{dI^{H,s}}{dt} = \underbrace{(1 - \xi) \rho E^H - \gamma I^{H,s}}_{\text{spreading dynamics}} - \underbrace{N_s^{\text{test}}}_{\text{testing}} - (1 - \xi) \left(\underbrace{\chi_{s,r} N^{\text{traced}}}_{\text{contact tracing}} - \underbrace{\frac{S}{M} \Phi_t}_{\text{ext. influx}} \right), \quad (6)$$

$$I^{H,a} = I^H - I^{H,s}, \quad (7)$$

$$\frac{dR}{dt} = \underbrace{\gamma(I^Q + I^H)}_{\text{recovered/removed individuals}}. \quad (8)$$

S1.6 Initial conditions

Let x be the vector collecting the variables of all different pools:

$$x = [S, E^Q, E^H, I^Q, I^H, I^{H,s}, R]. \quad (9)$$

We assume a population size of $M = 1e6$ individuals, so that $\sum_{i \neq 6} x_i = M$, and a prevalence of $I_0 = 200$ infections per million, so that $I^Q(0) = I_0$. Assuming that the hidden amount of infections is in the same order of magnitude I_0 , we would have $I^H(0) = I_0$, $I^{H,s}(0) = (1 - \xi)I_0$. We would expect the exposed individuals to scale with $(1 - k_t) R_0 I_0$, but we rather assume them to have the same size of the corresponding infectious pool. To calculate the initially susceptible individuals, we use $S(0) = 1 - \sum_{i \neq \{1,6\}} x_i$.

S1.7 Effect of delays and capacity limit on the effectiveness of TTI strategies

In this section we discuss further details on the derivation of the different parameters and variables involved in equations (1)–(8). First, as we assume contact tracing to be effective after a delay of τ days, some of the individuals who acquired the infection from those recently tested might have also become infectious by the time of tracing. Moreover, a fraction of those who became infectious might also have been tested by the tracing time, should they have developed symptoms.

Furthermore, we give explicit forms for N^{test} and N^{traced} , respectively, the number of cases identified exclusively by testing and contact-tracing, both for being within or over the TTI capacity. For simplicity, we assume that both testing and contact-tracing change their dynamics simultaneously, which depends on whether the daily amount of cases identified by testing N^{test} overpasses the TTI threshold $N_{\text{max}}^{\text{test}}$. After overwhelmed, the overhead testing would change its rate $\lambda_s \rightarrow \lambda'_s$, as only patients with a more specific set of symptoms would be tested. Nonetheless, the contact-tracing efforts can only follow the contacts of those $N_{\text{max}}^{\text{test}}$ observed cases, identifying a fraction η of the offspring infections they produced in their infectious period spent in unawareness of their state. The case of random testing is analyzed in the Supplementary Section 1.

S1.7.1 Limited testing capacity leading to lower testing rates

In the first stages of an outbreak, individuals with any symptoms from the broad spectrum of COVID-19-related symptoms would be tested, disregarding how specific those symptoms are. At this stage, we assume that the rate at which symptomatic individuals are tested is λ_s . Then, the number of individuals identified through testing (which, for simplicity is assumed to be solely symptom-driven) is given by

$$N_s^{\text{test}} = \lambda_s I^{H,s}. \quad (10)$$

When reaching the daily number $N_{\text{max}}^{\text{test}}$ of positive tests the testing capacity is reached. We then assume that further tests are only carried out for a more specific set of symptoms, leading to a smaller fraction of the population being tested. We therefore implement the testing capacity as a soft threshold. Assuming that after reaching $N_{\text{max}}^{\text{test}}$, the testing rate for further cases would decrease to λ'_s , the testing term N^{test} would be given by

$$N_s^{\text{test}} = \lambda_s \min(I^{H,s}, I_{\text{max}}^{H,s}) + \lambda'_s \max(0, I^{H,s} - I_{\text{max}}^{H,s}), \quad (11)$$

where $I_{\text{max}}^{H,s}$ represent the size of the infectious -symptomatic, hidden- pool i.e, $I_{\text{max}}^{H,s} = \frac{N_{\text{max}}^{\text{test}}}{\lambda_s}$.

S1.7.2 Modelling the number of traced individuals

To calculate the number of traced individuals, we assume that a fraction η of the newly tested individuals' contacts, and therefore their offspring infections, will be traced and subsequently quarantined. However these tested individuals stay on average a shorter amount of time in the infectious pool than the untested ones because they are quarantined, thus removed earlier from the pool. The number of offspring infections has therefore to be corrected by a factor: The average residence time in the infectious pool. For the case $\lambda_r = 0$, the average residence time is $\frac{1}{\gamma + \lambda_s}$, whereas the average residence time of untested individuals is $\frac{1}{\gamma}$. Dividing these two times gives us the wanted correction factor. The number of traced persons N^{traced} at time t is therefore:

$$N^{\text{traced}}(t) = \eta R_{t-\tau}^H \frac{\gamma}{\gamma + \lambda_s} N^{\text{test}}(t - \tau). \quad (12)$$

Otherwise, when the TTI capacity is overwhelmed, we assume that the number of traced individuals is limited, that only the contacts of N_{\max}^{test} individuals (already introduced in the previous section) can be traced:

$$N^{\text{traced}}(t) = \eta R_{t-\tau}^H \frac{\gamma}{\gamma + \lambda_s} N_{\max}^{\text{test}}. \quad (13)$$

S1.7.3 Individuals becoming infectious or being tested by the time of tracing

The traced individuals will be removed from either the exposed hidden pool E^H or from the infectious hidden pool I^H after the delay of τ days after testing. As we assume a tracing delay τ of only 2 days, a majority of the traced individuals would still be in exposed compartment. However, some might already become infectious by that time. To calculate the exact fraction of individuals remaining in the hidden exposed pool by the time of tracing, we proceed as follows. Let $s \in I_\tau = [0, \tau]$ be the time elapsed from the moment of testing. The emptying of the normalized exposed compartment (denoted \widetilde{E}^H) due to progression to the infectious stage would follow a first-order kinetics:

$$\frac{d\widetilde{E}^H}{ds} = -\rho \widetilde{E}^H, \quad \widetilde{E}^H(0) = 1 \quad (14)$$

The solution of (14) is given by $\widetilde{E}^H(s) = \exp(-\rho s)$. Therefore, we define χ_τ as the fraction of the traced individuals remaining in the E^H compartment at $s = \tau$:

$$\chi_\tau = \exp(-\rho\tau). \quad (15)$$

The remaining individuals are removed from the infectious compartment, which are then simply described by the fraction

$$\chi_r = 1 - \chi_\tau. \quad (16)$$

This however only holds for the asymptomatic hidden infectious pool. For the symptomatic hidden pool $I^{H,s}$, we do not want to remove the individuals which have already been tested, as they would be removed twice. For modelling the fraction of non-tested individuals remaining in the normalized symptomatic infectious compartment (denoted $\widetilde{I}^{H,s}$), we couple two first-order kinetics:

$$\frac{d\widetilde{I}^{H,s}}{ds} = \lambda_s \widetilde{I}^{H,s} + \rho \widetilde{E}^H, \quad \widetilde{I}^{H,s}(0) = 0. \quad (17)$$

The solution of (17) depends on whether $\lambda_s = \rho$ or not. The solution at $s = \tau$ which is the fraction of traced individuals removed from $I^{H,s}$ is given by:

$$\chi_{s,r} = \begin{cases} \rho\tau \exp(-\rho\tau) & \text{if } \lambda_s \approx \rho, \\ \frac{\rho}{\lambda_s - \rho} (\exp(-\rho\tau) - \exp(-\lambda_s\tau)) & \text{else.} \end{cases} \quad (18)$$

For the case $\lambda_r \neq 0$, the reader is referred to the Supplementary Note 4.

S1.8 Central epidemiological parameters that can be observed

In the real world, the disease spread can only be observed through testing and tracing. While the *true* number of daily infections N is a sum of all new infections in the hidden and traced pools, the *observed* number of daily infections \widehat{N}^{obs} is the number of new infections discovered by testing, tracing, and surveillance of the contacts of those individuals in the quarantined infectious pool I^Q , delayed by a variable reporting time. This includes internal contributions and contributions from testing and tracing:

$$N = \underbrace{\gamma(1 - k_t) R_0 \frac{S}{M} I^H}_{\text{hidden contagion}} + \underbrace{\gamma(\nu + \epsilon) R_0 \frac{S}{M} I^Q}_{\text{traced contagion}} + \underbrace{\frac{S}{M} \Phi_t}_{\text{ext. influx}} \quad (19)$$

$$\hat{N}^{\text{obs}} = \left[\underbrace{\rho E^Q}_{\text{traced contagion}} + \underbrace{N^{\text{test}} + (\chi_{s,r}(1 - \xi) + \chi_r \xi) N^{\text{traced}}}_{\text{TTI}} \right] \otimes \mathcal{K}, \quad (20)$$

where \otimes denotes a convolution and \mathcal{K} an empirical probability mass function that models a variable reporting delay, inferred from German data (as the RKI reports the date the test is performed, the delay until the appearance in the database can be inferred): The total delay between testing and reporting a test corresponds to one day more than the expected time the laboratory takes for obtaining results, which is defined as follows: from testing, 50% of the samples would be reported the next day, 30% the second day, 10% the third day, and further delays complete the remaining 10%, which for simplicity we will truncate at day four. Considering the extra day needed for reporting, the probability mass function for days 0 to 5 would be given by $\mathcal{K} = [0, 0, 0.5, 0.3, 0.1, 0.1]$. The spreading dynamics are usually characterized by the observed reproduction number \hat{R}_t^{obs} , which is calculated from the observed number of new cases $\hat{N}^{\text{obs}}(t)$. We here use the definition underlying the estimates that are published by Robert-Koch-Institute, the official body responsible for epidemiological control in Germany [60]: the reproduction number is the relative change of daily new cases N separated by 4 days (the assumed serial interval of COVID-19 [61]):

$$\hat{R}_t^{\text{obs}} = \frac{\hat{N}^{\text{obs}}(t)}{\hat{N}^{\text{obs}}(t - 4)} \quad (21)$$

In contrast to the original definition of \hat{R}_t^{obs} [60], we do not need to remove real-world noise effects by smoothing this ratio.

S1.9 Numerical calculation of solutions and critical values.

The numerical solution of the delay differential equations governing our model were obtained using a versatile solver that tracks discontinuities and integrates with the explicit Runge-Kutta (2,3) pair, `@dde23` implemented in MATLAB (version 2020a), with default settings. This algorithm allows the solution of non-stiff systems of differential equations in the shape $y'(t) = f(t, y(t), y(t - \tau_1), \dots, y(t - \tau_k))$, for a set of discrete lags $\{\tau_i\}_{i=1}^k$. Suitability and details on the algorithm are further discussed in [62].

To derive the tipping point between controlled and uncontrolled outbreaks (e.g. critical, minimal required contact reduction k_t^{crit} for both stability and metastability), and to plot the stability diagrams, we used the `@fzero` MATLAB function, and the linear approximation of the system of DDE (2)–(6) for the $\frac{S}{M} \approx 1$ limit. This function uses a combination of bisection, secant, and inverse quadratic interpolation methods to find the roots of a function. For instance, following the discussion of Supplementary Section 1, The different critical values for the contact reduction k_t^{crit} were determined by systematically solving the nonlinear eigenvalues problem for stability [63], where the solution operation was approximated with a Chebyshev differentiation matrix [64].

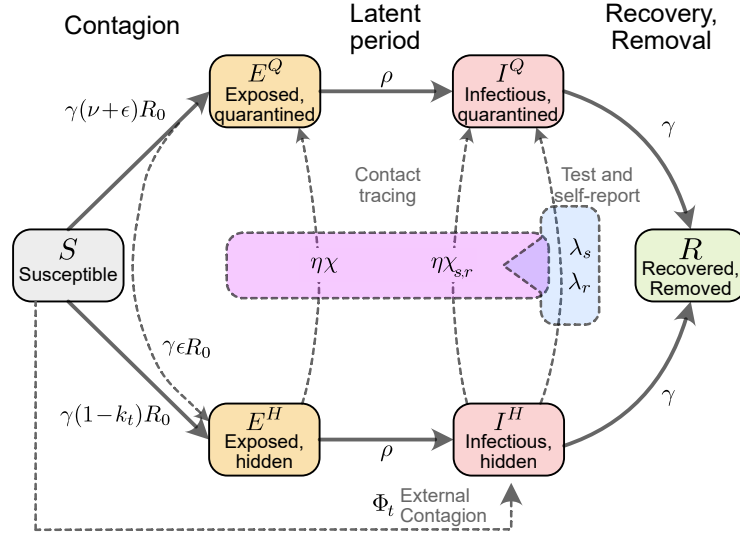
Supplementary Table S1: Model parameters.

Parameter	Meaning	Value (default)	Range	Units	Source
M	Population size	1 000 000		people	Assumed
R_0	Basic reproduction number	3.3	2.2–4.4	–	[14, 19, 20]
ν	Registered contacts (quarantined)	0.075		–	Assumed
ϵ	Lost contacts (quarantined)	0.05		–	Assumed
γ	Recovery/removal rate	0.10	0.08–0.12	day ⁻¹	[65–67]
ξ	Asymptomatic ratio	0.32	0.15–0.43	–	[15, 16, 55]
λ_s	Symptom-driven testing rate	0.25	0–1	day ⁻¹	Assumed
λ'_s	Symptom-driven testing rate (reduced capacity)	0.1		day ⁻¹	Assumed
η	Tracing efficiency	0.66		–	Assumed
τ	Contact tracing delay	2		days	Assumed
N_{\max}^{test}	Maximal tracing capacity	50	10–75	cases day ⁻¹	Assumed
Φ_t	External influx	1		cases day ⁻¹	Assumed
ρ	Exposed-to-infectious rate	0.25		day ⁻¹	[8, 68]
D_L	lockdown duration	4	0–8	weeks	Assumed
D_{ramp}	Phase-transition duration (lockdown)	1		weeks	Assumed
k_0	Baseline contact reduction	20 %		–	Assumed
k_{LD}	Contact reduction during lockdown	75 %		–	Assumed
k_{nLD}	Contact reduction post lockdown	40 %		–	Assumed
Φ_{LD}	Ext. influx (during lockdown)	0.1		cases day ⁻¹	Assumed
Φ_{nLD}	Ext. influx (post lockdown)	1		cases day ⁻¹	Assumed
χ_τ	Fraction of contacts traced before becoming infectious	0.61		–	eq (15)
$\chi_{s,r}$	Fraction of contacts traced after becoming infectious, before being tested (symptomatic and random)	0.30		–	eq (18)
χ_r	Fraction of contacts traced after becoming infectious, before being tested (random)	0.39		–	eq (16)

Supplementary Table S2: Model variables.

Variable	Meaning	Units	Explanation
S	Susceptible pool	people	non-infected people that may acquire the virus.
E^Q	Exposed pool (quarantined)	people	Total quarantined exposed people.
E^H	Exposed pool (hidden)	people	Total non-traced, non-quarantined exposed people.
$I^{H,s}$	Infectious pool (hidden, symptomatic)	people	Non-traced, non-quarantined people who are symptomatic.
I^H	Infectious pool (hidden)	people	Total non-traced, non-quarantined infectious people.
I^Q	Infectious pool (quarantined)	people	Total quarantined infectious people.
N	New infections (Total)	cases day ⁻¹	Given by: $N = \gamma(1 - k_t) R_0 I^H + \gamma(\nu + \epsilon) R_0 I^Q + \frac{S}{M} \Phi_t$.
k_t	Contact reduction	%	Reduction of infectious contacts, related to pre-COVID-19 times.
\hat{N}^{obs}	Observed new infections (influx to traced pool)	cases day ⁻¹	Daily new cases, observed from the quarantined pool; delayed because of imperfect reporting and realistic contact tracing.
\hat{R}_t^{obs}	Observed reproduction number	–	The reproduction number that can be estimated only from the observed cases: $\hat{R}_t^{\text{obs}} = \hat{N}^{\text{obs}}(t) / \hat{N}^{\text{obs}}(t - 4)$.

S2 Supplementary Notes



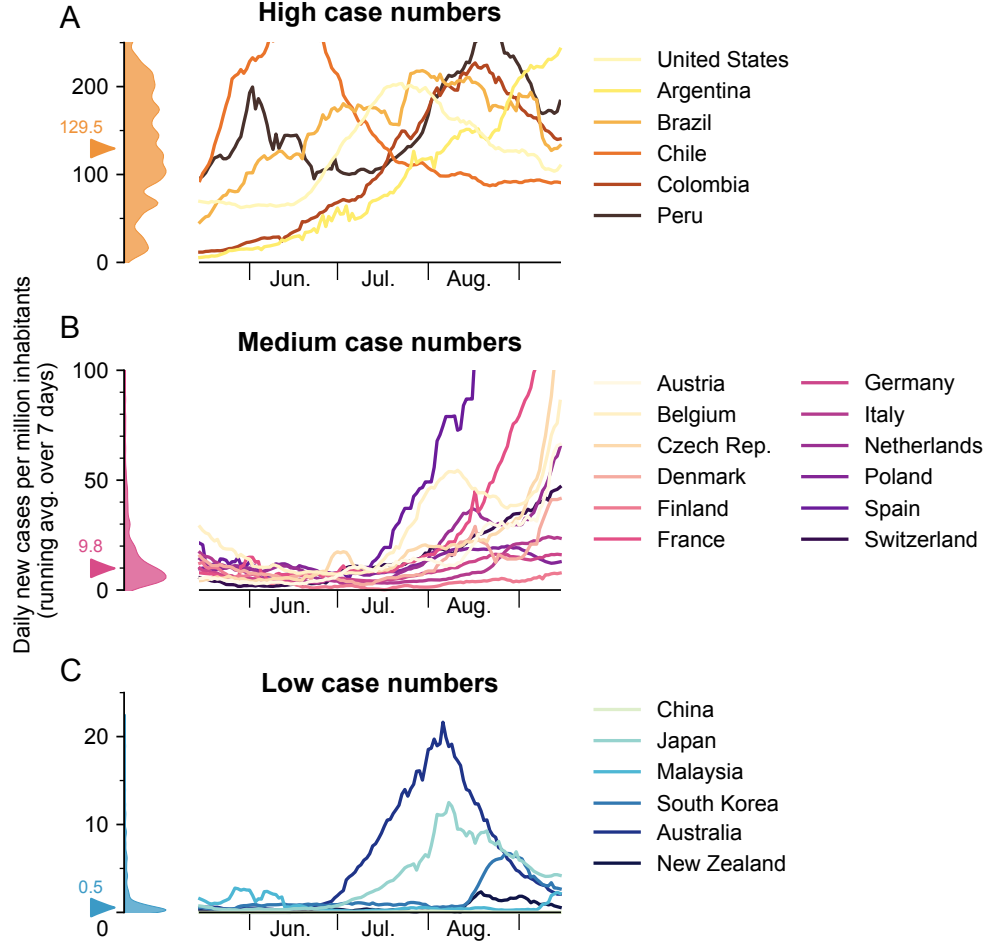
Supplementary Figure S1: **Flowchart of the complete model.**

S2.1 Strategies to face COVID-19 differ among countries.

Very low case numbers and even local eradication has been achieved by several South- and East-Asian countries, as well as Australia and New-Zealand. By aiming for local eradication, these countries reached very low values below one daily new case per million (median 0.5, Fig. S2 C). If local eradication is successful, these countries can profit from the absorbing state of zero SARS-CoV-2 infections, i.e. after local eradication new infection chains are only started if a virus is *de novo* carried into the country [69, 70]. However, the local eradication is constantly put at risk by undetected influx of new viruses from abroad, requiring very strict quarantine for international travel, and – once the spread got out of control – decisive action to completely stop all infection chains. However, the more countries adhere to this strategy successfully, the closer one may get to global eradication.

In many European countries over the summer, case numbers were relatively low, typically around 10 daily new cases per million (Fig. S2 B). During that time, contacts were in general only mildly or moderately restricted, and containment was complemented by hygiene, masks, and other preventive measures. However, in summer and autumn, most European countries developed a second wave Fig. S4. The causes are certainly diverse, from increasing contact rates to seasonal effects and travel-related influx. Seasonal effects alone cannot explain the second wave, as neighboring countries like Portugal versus Spain, or Finland versus Sweden show greatly different dynamics (see [52]). Hence, it seems to be possible to maintain an equilibrium at fairly low case numbers, but that equilibrium is fragile at high case numbers and novel waves can emerge at any time.

Sustained high levels of case numbers have been observed in several countries such that TTI probably couldn't be performed effectively. Around 130 daily new cases per million have been observed e.g. in many (but not all) American countries (median 129.54, Fig. S2 A). It shows that high levels of daily new infections can be maintained in principle. However the stringency of interventions is similar or higher compared to other countries (see [40]), and even with these high numbers it will probably take about $200.000/150 = 1333$ to $700.000/150 = 4666$ days, thus several years, until 20 to 70% of the population is infected and herd immunity reached – assuming the duration of individual immunity is long enough. That high level of new infections leads to a considerable death toll, as currently about 1.5% of the infected would die (depending on age structure [71, 72]). Moreover, containment measures like quarantine become unsustainable because, if implemented, each one of the 200 daily new infected cases would require the quarantine of 5-50 people (their high-risk contacts) for about 10 days, causing 1 - 10% of the population being in quarantine at any given day. Therefore the alleged economical and social benefits of such a strategy [73, 74] may be questionable.



Supplementary Figure S2: **Strategies of countries to fight SARS-CoV-2 differ widely and are reflected in case numbers.** (A) Strategies that involve little nonpharmaceutical interventions rely on the population to hinder the spread in a self-regulated manner and are often accompanied by high case numbers. Examples can be dominantly found in North- and South-America, the median of daily new cases for the shown examples and time range exceeds 100 per million inhabitants per day. (B) Strategies that aim to keep case numbers low through extensive TTI, combined with temporary lockdowns can lead to medium case numbers. As the effectiveness of TTI measures depends on daily infections, case numbers can seemingly explode when the (hard-to-estimate) TTI capacity limit is exceeded. Many European countries managed to stabilize case numbers over the summer but are now seeing case numbers that rise faster-than-exponential. The median of daily new cases for the shown examples and time range is 9.88 per million per day. (C) When the external influx is low and/or employed strategies to reduce contacts are very effective, the stable regime can be reached. In this case, average case numbers are very low and local outbreaks can be controlled well through local interventions. Examples can be dominantly found in East-Asia and Oceania. The median of daily new cases for the shown examples and time range is 0.55 per million per day. Raw data and preliminary visualizations were obtained from [52].

S2.2 On the incorporation of random testing in the TTI scheme

Testing can also be done in a random manner or randomly combined with a tracing strategy. Even though the amount of tests that would be required for such purposes would be enormous, the development of fast, cheap, and reliable tests offers an interesting alternative to consider.

In this supplementary note we derive the equations presented in the methods but also including random testing. As therein described, random testing is assumed to occur at a constant rate λ_r , which, for default parameters, reflect the amount of tests per day per million people. In that way, it seems reasonable to consider unfeasible testing rates surpassing $\lambda_r^{\max} = 0.1$, as it would mean that a 10% of the population is tested everyday.

S2.2.1 Number of cases observable through testing N^{test}

When random testing is included in the scheme, the solution of equation (17) for the symptomatic and asymptomatic infections -hidden- would be given by equations (22) and (23).

$$\chi_{s,r} = \begin{cases} \rho\tau \exp(-\rho\tau), & \text{if } \rho \approx \lambda_s + \lambda_r \\ \frac{\rho}{(\lambda_s + \lambda_r) - \rho} (\exp(-\rho\tau) - \exp(-\tau(\lambda_s + \lambda_r))), & \text{else.} \end{cases} \quad (22)$$

$$\chi_r = \begin{cases} \rho\tau \exp(-\rho\tau), & \text{if } \rho \approx \lambda_r \\ \frac{\rho}{\lambda_r - \rho} (\exp(-\rho\tau) - \exp(-\tau\lambda_r)), & \text{else.} \end{cases} \quad (23)$$

If both symptom-based and random testing take place simultaneously, the number of discovered infections is given by

$$N^{\text{test}} = \lambda_r I^H + \lambda_s I^{H,s} \quad (24)$$

Further, assuming that after reaching $N_{\text{max}}^{\text{test}}$, the testing rates at the overhead pool-sizes would decrease to λ'_s and λ'_r , respectively, for symptom-driven and random testing. We further assume that testing resources would be exclusively allocated to sustain the symptom-driven testing in our default scenario. The overall testing term N^{test} would be given by:

$$N^{\text{test}} = \lambda_r \min(I^H, I_{\text{max}}^H) + \lambda'_r \max(0, I^H - I_{\text{max}}^H) + \lambda_s \min(I^{H,s}, I_{\text{max}}^{H,s}) + \lambda'_s \max(0, I^{H,s} - I_{\text{max}}^{H,s}), \quad (25)$$

where $I_{\text{max}}^{H,s}, I_{\text{max}}^H$ represent the pool sizes of the symptomatic hidden and total hidden pools, respectively, at the TTI limit, i.e. $\lambda_r I_{\text{max}}^H + \lambda_s I_{\text{max}}^{H,s} \stackrel{!}{=} N_{\text{max}}^{\text{test}}$, reached at time $t = t^*$. Defining $\varphi := \frac{I^{H,s}}{I^H} \Big|_{t=t^*}$, we can express such magnitudes in term of the maximum capacity $N_{\text{max}}^{\text{test}}$:

$$I_{\text{max}}^{H,s} = \frac{\varphi N_{\text{max}}^{\text{test}}}{\varphi \lambda_s + \lambda_r} \quad (26)$$

$$I_{\text{max}}^H = \frac{N_{\text{max}}^{\text{test}}}{\varphi \lambda_s + \lambda_r}. \quad (27)$$

The explicit value of φ can be obtained numerically in the integration routine, or estimated through the use of the equilibrium values of the differential equations, $\varphi = \frac{I_{\infty}^{H,s}}{I_{\infty}^H}$ (as implemented in our code). The expression for the symptomatic hidden pool $I^{H,s}$ in the presence of random testing is slightly different;

$$N_s^{\text{test}} = \lambda_r \min(I^{H,s}, I_{\text{max}}^{H,s}) + \lambda'_r \max(0, I^{H,s} - I_{\text{max}}^{H,s}) + \lambda_s \min(I^{H,s}, I_{\text{max}}^{H,s}) + \lambda'_s \max(0, I^{H,s} - I_{\text{max}}^{H,s}). \quad (28)$$

S2.2.2 Number of cases observable through contact-tracing N^{traced}

Because of TTI, infectious individuals move (or are likely to move) from the hidden to the quarantined infectious pool before recovering. Therefore, they spend a comparatively shorter amount of time there and, on average, would not generate the expected amount of offspring infections as some would be prevented. Assuming the average residence time of untested individuals is $\frac{1}{\gamma}$, we estimate the residence time of individuals removed by symptom-driven testing and random testing. Noting that symptomatic individuals can be tested and therefore removed by any of the testing criteria, their residence time would be approximately $\frac{1}{\gamma + \lambda_s + \lambda_r}$, whereas the average residence time of asymptomatic individuals would be $\frac{1}{\gamma + \lambda_r}$. Therefore, the fractions of time that symptomatic and asymptomatic individuals stay unnoticed are respectively

$$t_s = \frac{\gamma}{\gamma + \lambda_s + \lambda_r}, \quad (29)$$

and

$$t_r = \frac{\gamma}{\gamma + \lambda_r}. \quad (30)$$

If the daily new cases observed through testing, delayed at the moment of processing, $N_{t-\tau}^{\text{test}}$, are within the tracing capacity of the health authorities, i.e. $N_{t-\tau}^{\text{test}} \leq N_{\text{max}}^{\text{test}}$, then N^{traced} is defined as

$$N^{\text{traced}} = \eta R_{t-\tau}^H \left(I_{t-\tau}^H t_r \lambda_r + I_{t-\tau}^{H,s} (t_s \lambda_s + (t_s - t_r) \lambda_r) \right). \quad (31)$$

Otherwise, using the expressions for I^H and $I^{H,s}$ when the TTI capacity is reached derived in the previous section, we can obtain an effective rate

$$\lambda_{\text{eq}} = \frac{\lambda_r (1 - \varphi) t_r + \varphi \lambda_s t_s}{\lambda_r + \varphi \lambda_s}. \quad (32)$$

Therefore, the average amount of positive cases identified by contact tracing in the TTI limit is given by

$$N^{\text{traced}} = \eta R_{t-\tau}^H N_{\text{max}}^{\text{test}} \lambda_{\text{eq}}. \quad (33)$$

To sum up the last equations:

$$N^{\text{traced}} = \begin{cases} \eta R_{t-\tau}^H (I_{t-\tau}^H t_r \lambda_r + I_{t-\tau}^{H,s} (t_s \lambda_s + (t_s - t_r) \lambda_r)) & \text{if } N_{t-\tau}^{\text{test}} \leq N_{\text{max}}^{\text{test}} \\ \eta R_{t-\tau}^H N_{\text{max}}^{\text{test}} \lambda_{\text{eq}} & \text{else} \end{cases} \quad (34)$$

S2.3 Linear stability analysis and uncertainty propagation

For analyzing the stability of the governing differential equations, namely, whether an outbreak could be controlled, we studied the linear stability of the system. Moreover, we consider that, within the time-frame considered for stability purposes, the fraction $\frac{S}{M}$ would remain somewhat constant, we consider the linealized version of equations (2)– (6), defining a system of delay differential equations for the variables $x(t) = [E^Q(t); E^H(t); I^Q(t); I^H(t); I^{H,s}(t)]$. We define matrices A and B as:

$$A = \begin{pmatrix} -\rho & 0 & \nu \gamma R_0 & 0 & 0 \\ 0 & -\rho & \epsilon \gamma R_0 & \gamma (1 - k_t) R_0 & 0 \\ \rho & 0 & -\gamma & \lambda_r & \lambda_s \\ 0 & \rho & 0 & -\gamma - \lambda_r & -\lambda_s \\ 0 & (1 - \xi) \rho & 0 & 0 & -\gamma - \lambda_r - \lambda_s \end{pmatrix} \quad (35)$$

$$B = \begin{pmatrix} 0 & 0 & 0 & \lambda_r^{\text{eff}} \chi_\tau & \lambda_s^{\text{eff}} \chi_\tau \\ 0 & 0 & 0 & -\lambda_r^{\text{eff}} \chi_\tau & -\lambda_s^{\text{eff}} \chi_\tau \\ 0 & 0 & 0 & \lambda_r^{\text{eff}} (\xi \chi_r + (1 - \xi) \chi_{s,r}) & \lambda_s^{\text{eff}} (\xi \chi_r + (1 - \xi) \chi_{s,r}) \\ 0 & 0 & 0 & -\lambda_r^{\text{eff}} (\xi \chi_r + (1 - \xi) \chi_{s,r}) & -\lambda_s^{\text{eff}} (\xi \chi_r + (1 - \xi) \chi_{s,r}) \\ 0 & 0 & 0 & -\lambda_r^{\text{eff}} (1 - \xi) \chi_{s,r} & -\lambda_s^{\text{eff}} (1 - \xi) \chi_{s,r} \end{pmatrix} \eta (1 - k_t) R_0, \quad (36)$$

where

$$\lambda_r^{\text{eff}} = \frac{\gamma \lambda_r}{\lambda_r + \gamma}, \quad \lambda_s^{\text{eff}} = \gamma \left(\frac{\lambda_s + \lambda_r}{\gamma + \lambda_s + \lambda_r} - \frac{\lambda_r}{\lambda_r + \gamma} \right). \quad (37)$$

The equations governing the dynamics for vector $x(t)$ are then presented in their matrix form:

$$x'(t) = Ax(t) + Bx(t - \tau). \quad (38)$$

We determine the critical values for the contact reduction k_t^{crit} , for which exponential solutions would be asymptotically stable. Eigenvalues were determined by systematically solving the nonlinear eigenvalues

problem for stability [63], where the solution operation was approximated with a Chebyshev differentiation matrix [64]. Eigenvalues, in this sense, would be solutions of the scalar equation

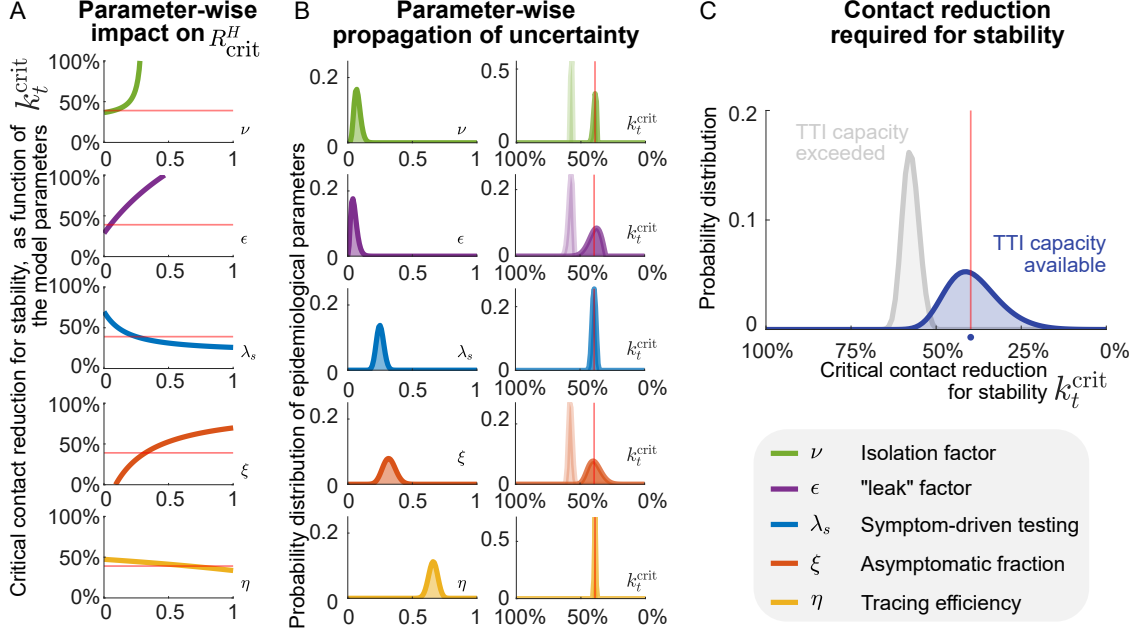
$$\det(-sI + A + e^{-s\tau}B) = 0 \quad (39)$$

Noting that A and B explicitly depend on the model parameters, we numerically explore which combinations of them would result in stable, metastable or unstable case numbers. Concretely, we studied the minimum –critical– contact reduction required for stabilization k_t^{crit} in two scenarios; i) low case numbers, and TTI fully operative (both testing and contact tracing), and ii) high case numbers, above the TTI limit, where testing would be inefficient and solely symptom driven ($\lambda_s = \lambda'_s$, $\eta = \lambda_r = \lambda'_r = 0$).

To explore the uni-variate impact different signature parameters have on k_t^{crit} , we studied the zeros of (39) as a function of k_t using the `@fzero` MATLAB function (Fig. S3A). Using the same routines and a random sampling procedure, we propagate uncertainties in the values of these parameters, uni-variate (Fig. S3B), and multivariate (Fig. S3C).

Supplementary Table S3: Parameter uncertainty propagation

Parameter	Meaning	Median	95% CI	α	β	Dist.	Units
ξ	Asymptomatic ratio	0.32	0.23–0.42	27.5	27.8	beta	–
λ_s	Symptom-driven test rate	0.25	0.20–0.31	56	168	beta	days ⁻¹
ν	Registered contacts (quarantined)	0.07	0.03–0.13	8.25	101.8	beta	–
η	Tracing efficiency	0.66	0.59–0.73	117.9	60.7	beta	–
ϵ	Lost contacts (quarantined)	0.05	0.01–0.11	3.8	71.25	beta	–
$k_t^{\text{crit}} \Big _{\text{TTI}}$	Necessary contact reduction with TTI	39 %	24–53 %	–	–	–	–
$k_t^{\text{crit}} \Big _{\text{no TTI}}$	Necessary contact reduction without TTI	58 %	53–62 %	–	–	–	–



Supplementary Figure S3: **Propagation of TTI-parameter uncertainties to the critical contact reduction required for stability.** As the different parameters involved in our model play different roles, the way their variability propagates to k_t^{crit} differs, even when their variability profiles look similar. **(A)** Impact of single-parameter variation on the critical hidden reproduction number k_t^{crit} . To evaluate the monotony (direction) of their impact on k_t^{crit} , we scan their entire definition range, ignoring the practical feasibility of achieving such values. Dotted black line shows the default critical hidden reproduction number. **(B)** Univariate uncertainties of TTI parameters modelled by beta distributions centered on their default value (dotted black line), and the resulting distribution of critical reproduction numbers k_t^{crit} (right column). Results are shown assuming testing only (light colors) or testing and tracing (dark colors). The default value of k_t^{crit} is marked by the dotted lines, in the presence (black) or absence (grey) of tracing. **(C)** Distribution of critical reproduction numbers arising from multivariate uncertainty propagation given by the joint of the distributions shown in (A) for testing only (light colors), or testing and tracing (dark colors). The default value of R_{crit}^H is marked by the dotted lines, in the presence (black) or absence (grey) of tracing. Results show averages of 100 000 realizations.

On the contact reduction required for achieving early herd immunity.

In Supplementary Section S2.3, we derived a methodology for obtaining the minimal, critical contact reduction k_t^{crit} for which the linear system is asymptotically stable. Such values, however, assume a fully susceptible population, as we ignore the scaling factor $\frac{S}{M}$.

The herd immunity threshold ϱ represents the fraction of the population that needs to be immunized for controlling the spread of an infectious disease. It can be expressed in terms of the effective reproduction number R_t :

$$\varrho = 1 - \frac{1}{R_t}. \quad (40)$$

In the context of our model, R_t can be expressed in terms of the reduction of contagious contacts k_t and the basic reproduction number R_0 ; $R_t = (1 - k_t) R_0$. Nonetheless, in further stages of an ongoing outbreak, the fraction of people that is no longer susceptible would have an effect, thus we include also the scaling factor $\frac{S}{M}$:

$$R_t = (1 - k_t) \frac{S}{M} R_0. \quad (41)$$

Combining both equation (40) and (41), we can express ϱ as

$$\varrho = 1 - \frac{1}{(1 - k_t)(1 - f)R_0}, \quad (42)$$

assuming a quasi-stationary dynamics for S , and defining $f = 1 - \frac{S}{M}$. Suppose we study the case in which no major behavioral changes take place, thus the herd immunity threshold ϱ would remain the same. On the other hand, because of the sole fact of having a progressively increasing immunization among the population (because of vaccination or post-infection immunity), the required reduction of contacts for stabilization k_t^{crit} will decrease. Assuming critical conditions, we use $k_t = k_t^{\text{crit}}$ in equation (42):

$$\varrho = 1 - \frac{1}{(1 - k_t^{\text{crit}})(1 - f)R_0}, \quad (43)$$

As we assumed that no behavioral change is taking place, we obtain the herd immunity threshold by only evaluating equation (40) at $f = 0$.

$$\varrho = 1 - \frac{1}{(1 - k^{\text{crit},0})R_0}, \quad (44)$$

and subtracting (43) and (44) we obtain an expression for $k_t^{\text{crit}}(f)$

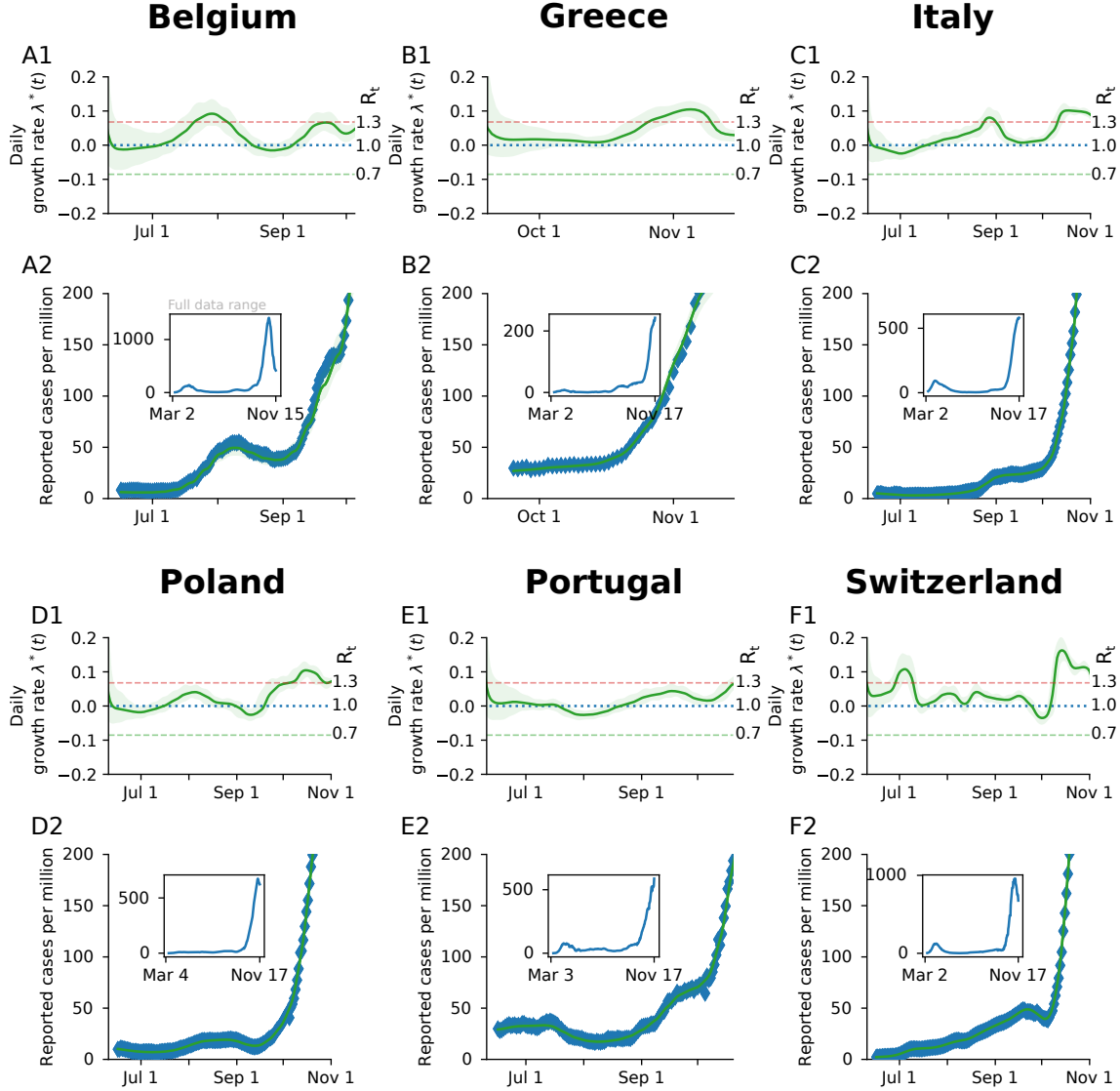
$$k_t^{\text{crit}}(f) = 1 - \frac{1 - k^{\text{crit},0}}{1 - f} \quad (45)$$

Inferring the reproduction number of COVID-19 from Jun to Oct. 2020

We use the framework of Bayesian inference on an SIR model presented in our previous work [39] to infer the daily growth rate $\lambda^*(t)$. An SIR compartmental model with weekly change points is used whose central epidemiological parameters are inferred using the PyMC3 package [75]. A weekly modulation was applied to take weekly reporting structure and weekend delays into account. After inference a rolling average was performed on the daily case numbers for comparability and clarity. The effective reproduction number \hat{R}_t^{eff} can be expressed dependent on the effective daily growth rate:

$$\hat{R}_t^{\text{eff}} = (\lambda^*(t) + 1)^4 \quad (46)$$

This short analysis was performed for Germany (Fig. 6) and other European countries (Fig. S4) which showed the same metastable behaviour, while their case numbers were below a threshold around 50 cases per day (per million). A transition into the unstable regime can be seen once case numbers surpass this threshold.



Supplementary Figure S4: **Comparison of the reproduction number and reported cases as second wave emerges in different European countries.** For each country, parameters of an SIR model were fitted to the reported data of the Our World in Data repository [52], following the procedure presented in [39]. (**Panels X1**) The time-dependent effective growth rate stays between -0.1 and 0.1 and rises before the tipping point. This corresponds to an effective reproduction number between 0.7 and 1.3 , which matches our preliminary assumptions. The time range is adjusted to focus on the tipping point. (**Panels X2**) After a (meta-)stable regime in summer, all of the selected countries show a rise in case numbers and a tipping point at around 50 new cases per day per million, where the spread self-accelerates and the cases increase significantly. (**Insets**) Case numbers for the full available time range.